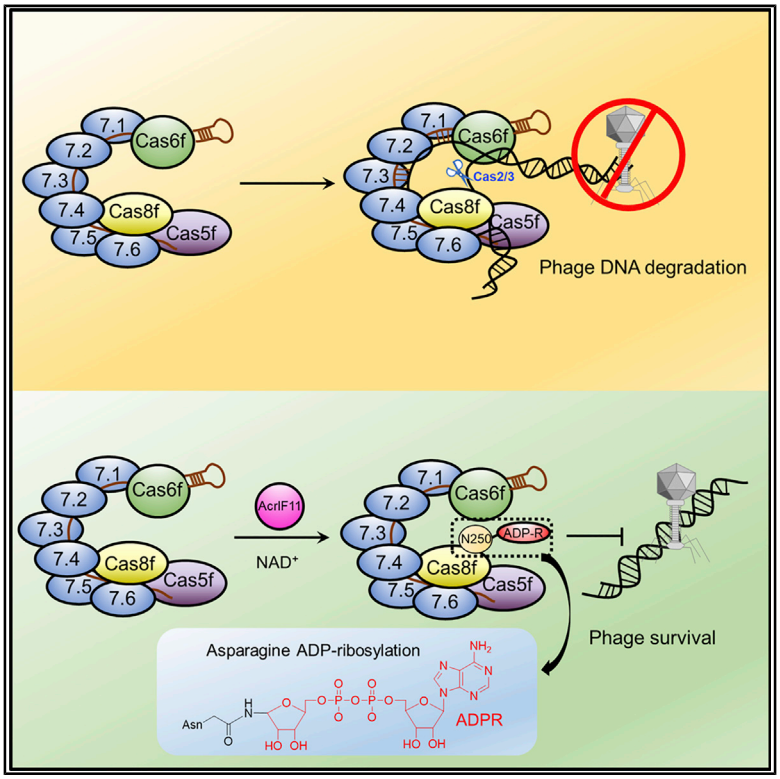
Molecular Cell

Article

# A Type I-F Anti-CRISPR Protein Inhibits the CRISPR-Cas Surveillance Complex by ADP-Ribosylation

## Graphical Abstract




## Highlights

- Crystal structure of AcrIF11 suggests that it resembles an ADP-ribosyltransferase
- AcrIF11 specifically ADP-ribosylates a key residue in the PAM-recognition loop
- AcrIF11-mediated ADP-ribosylation of the Csy complex prevents dsDNA binding
- AcrIF11 requires the Cas7.6f subunit for binding to and modifying the Csy complex

## Authors

Yiying Niu, Lingguang Yang, Teng Gao, ..., Yi Zhang, Xiaoyun Liu, Yue Feng

## Correspondence

zeliangchen@yahoo.com (Z.C.), zhangyishirly@hotmail.com (Y.Z.), xiaoyun.liu@bjmu.edu.cn (X.L.), fengyue@mail.buct.edu.cn (Y.F.)

## In Brief

Niu et al. report structural and biochemical data that reveal the molecular mechanism of AcrIF11-mediated inhibition of the type I-F CRISPR system. AcrIF11 specifically ADP-ribosylates a key residue in the PAM-recognition loop of the type I-F Cascade complex, thereby inhibiting its DNA binding activity and inactivating the CRISPR system.

Niu et al., 2020, Molecular Cell *80*, 1–13
November 5, 2020 © 2020 Elsevier Inc.
https://doi.org/10.1016/j.molcel.2020.09.015

CellPress

Please cite this article in press as: Niu et al., A Type I-F Anti-CRISPR Protein Inhibits the CRISPR-Cas Surveillance Complex by ADP-Ribosylation, Molecular Cell (2020), https://doi.org/10.1016/j.molcel.2020.09.015

Molecular Cell

CellPress

Article

# A Type I-F Anti-CRISPR Protein Inhibits the CRISPR-Cas Surveillance Complex by ADP-Ribosylation

Yiying Niu,[1,11] Lingguang Yang,[1,11] Teng Gao,[1,11] Changpeng Dong,[2,11] Buyu Zhang,[3,11] Peipei Yin,[1] Ann-Katrin Hopp,[4] Dongdong Li,[5] Rui Gan,[6] Hongou Wang,[7] Xi Liu,[1] Xueli Cao,[1] Yongchao Xie,[1] Xianbin Meng,[8] Haiteng Deng,[8] Xiaohui Zhang,[9] Jie Ren,[10] Michael O. Hottiger,[4] Zeliang Chen,[1,2,*] Yi Zhang,[1,*] Xiaoyun Liu,[7,*] and Yue Feng[1,12,*]

[1]Beijing Advanced Innovation Center for Soft Matter Science and Engineering, Beijing Key Laboratory of Bioprocess, State Key Laboratory of Chemical Resource Engineering, College of Life Science and Technology, Beijing University of Chemical Technology, Beijing 100029, China

[2]Key Laboratory of Livestock Infectious Diseases in Northeast China, Ministry of Education, College of Animal Science and Veterinary Medicine, Shenyang Agricultural University, Liaoning Province, Shenyang 110866, China

[3]Institute of Analytical Chemistry, College of Chemistry and Molecular Engineering, Peking University, Beijing 100871, China

[4]Department of Molecular Mechanisms of Disease, University of Zurich, 8057 Zurich, Switzerland

[5]The Protein Preparation and Characterization Core Facility of Tsinghua University, The China National Center for Protein Sciences (Beijing) Tsinghua University Branch, Beijing 100084, China

[6]HIT Center for Life Sciences, School of Life Science and Technology, Harbin Institute of Technology, Harbin 150080, China

[7]Department of Microbiology, School of Basic Medical Sciences, Peking University Health Science Center, Beijing 100191, China

[8]MOE Key Laboratory of Bioinformatics, School of Life Sciences, Tsinghua University, Beijing 100084, China

[9]State Key Laboratory of Natural and Biomimetic Drugs, Peking University, 38 Xueyuan Road, Beijing 100191, China

[10]State Key Laboratory for Biology of Plant Diseases and Insect Pests/Key Laboratory of Control of Biological Hazard Factors (Plant Origin) for Agri-product Quality and Safety, Ministry of Agriculture, Institute of Plant Protection, Chinese Academy of Agricultural Sciences, Beijing 100081, China

[11]These authors contributed equally

[12]Lead Contact

*Correspondence: zeliangchen@yahoo.com (Z.C.), zhangyishirly@hotmail.com (Y.Z.), xiaoyun.liu@bjmu.edu.cn (X.L.), fengyue@mail.buct.edu.cn (Y.F.)

https://doi.org/10.1016/j.molcel.2020.09.015

## SUMMARY

CRISPR-Cas systems are bacterial anti-viral systems, and phages use anti-CRISPR proteins (Acrs) to inactivate these systems. Here, we report a novel mechanism by which AcrIF11 inhibits the type I-F CRISPR system. Our structural and biochemical studies demonstrate that AcrIF11 functions as a novel mono-ADP-ribosyltransferase (mART) to modify N250 of the Cas8f subunit, a residue required for recognition of the protospacer-adjacent motif, within the crRNA-guided surveillance (Csy) complex from *Pseudomonas aeruginosa*. The AcrIF11-mediated ADP-ribosylation of the Csy complex results in complete loss of its double-stranded DNA (dsDNA) binding activity. Biochemical studies show that AcrIF11 requires, besides Cas8f, the Cas7.6f subunit for binding to and modifying the Csy complex. Our study not only reveals an unprecedented mechanism of type I CRISPR-Cas inhibition and the evolutionary arms race between phages and bacteria but also suggests an approach for designing highly potent regulatory tools in the future applications of type I CRISPR-Cas systems.

## INTRODUCTION

CRISPR-Cas systems are part of the prokaryotic adaptive immune system against foreign genetic elements, including invading viruses (Marraffini, 2015; van der Oost et al., 2014). They are divided into class 1 systems, which deploy multi-subunit surveillance complexes guided by CRISPR RNA (crRNA), and class 2 systems, which depend on crRNA-guided single-subunit Cas proteins. The two classes are further divided into 6 types (types I–VI) and 19 subtypes (Makarova et al., 2015). The type I multi-subunit CRISPR-Cas system is the most ubiquitous and largest in molecular size, and it is further divided into seven subtypes: I-A through I-F and I-U. All type I systems deploy multi-subunit crRNA-guided surveillance complexes to identify foreign DNA, which is degraded by the *trans*-acting nuclease-helicase Cas3 (Cas2/3 in type I-F). The type I-F system of *Pseudomonas aeruginosa* encodes a 350-kDa crRNA-guided surveillance complex (i.e., the Csy complex) composed of nine Cas proteins (one Cas5f, one Cas8f, one Cas6f, and six Cas7f proteins) and a single 60-nt crRNA (Chowdhury et al., 2017; Guo et al., 2017; Peng

Please cite this article in press as: Niu et al., A Type I-F Anti-CRISPR Protein Inhibits the CRISPR-Cas Surveillance Complex by ADP-Ribosylation, Molecular Cell (2020), https://doi.org/10.1016/j.molcel.2020.09.015



et al., 2017; Rollins et al., 2019). The complex is assembled into an asymmetric spiral, in which the crRNA is largely extended, allowing direct interaction with all nine protein subunits. In the head region, Cas6f (formerly Csy4) is stably associated with the 3′ end of the crRNA after cleaving it at the stem-loop structures consisting of palindromic repeat sequences (Haurwitz et al., 2010; Przybilski et al., 2011). Six Cas7f (formerly Csy3) subunits assemble along the crRNA, forming the backbone of the complex. In the tail region, the 5′ handle of the crRNA is anchored by extensive interactions with a stable heterodimer composed of Cas5f (formerly Csy2) and Cas8f (formerly Csy1) (Chowdhury et al., 2017; Guo et al., 2017; Peng et al., 2017; Rollins et al., 2019).

To effectively evade CRISPR systems, bacteriophages have evolved protein-based inhibitors, called anti-CRISPRs (Acrs), to inactivate the CRISPR-Cas immune systems (Koonin and Makarova, 2018; Marino et al., 2020; Pawluk et al., 2018). Studies have identified a large number of Acrs, targeting type I (Bondy-Denomy et al., 2013; He et al., 2018; Marino et al., 2018; Pawluk et al., 2014, 2016b), type II (Gussow et al., 2020; Eitzinger et al., 2020; Forsberg et al., 2019; Harrington et al., 2017; Hynes et al., 2017, 2018; Lee et al., 2018; Liu et al., 2019; Mahendra et al., 2020; Pawluk et al., 2016a; Rauch et al., 2017; Uribe et al., 2019; Watters et al., 2020), type III (Athukoralage et al., 2020; Bhoobalan-Chitty et al., 2019), type V (Marino et al., 2018; Watters et al., 2018), and recently type VI (Lin et al., 2020) CRISPR-Cas systems. For the type I CRISPR systems, 14 Acrs were described to target the type I-F system (i.e., AcrIF1-IF14), 7 Acrs were found to exclusively target the type I-E system (i.e., AcrIE1-IE7), 1 Acr targeted type I-C (i.e., AcrIC1), and 1 Acr targeted type I-D (i.e., AcrID1) (Hwang and Maxwell, 2019). AcrIF6 and fusion protein AcrIE4-F7 could target both type I-E and type I-F systems (Marino et al., 2018; Pawluk et al., 2016b). Despite the growing number of identified Acr proteins, the working mechanisms of only a few of them have been characterized in detail. The structural basis underlying the mechanisms of type I-F Acrs has been determined for AcrIF1, AcrIF2 (Chowdhury et al., 2017; Guo et al., 2017; Peng et al., 2017), AcrIF3 (Rollins et al., 2019; Wang et al., 2016a, 2016b), and AcrIF10 (Guo et al., 2017). During the preparation of our manuscript, the structures of AcrIF6/8/9 complexed with the Csy complex were also reported (Zhang et al., 2020). All of these Acrs inhibit the type I-F system through direct interactions with either the Csy complex (AcrIF1/2/4/6/8/9/10) or the Cas2/3 helicase-nuclease (AcrIF3). They inactivate the CRISPR system either by disrupting DNA binding (AcrIF1/2/6/8/9/10) or by inhibiting target sequence cleavage (AcrIF3). Given the diverse sequences of Acr proteins, it is important to investigate whether novel strategies are used by other Acr proteins.

Here, we elucidate the mechanism of how AcrIF11 inactivates the type I-F CRISPR system. The biochemical and structural data revealed that AcrIF11 functions as a novel mono-ADP-ribosyltransferase (mART) that modifies N250 of the Cas8f subunit within the Csy complex from *P. aeruginosa*, a residue that is required for the recognition of the protospacer-adjacent motif (PAM). It has been reported that type I CRISPR-Cas systems could be used for long-range genome manipulations and expression modulations of targeted endogenous genes in human cells (Dolan et al., 2019; Pickar-Oliver et al., 2019). Therefore, our results not only reveal an unprecedented mechanism for inactivating the type I multi-subunit CRISPR complexes but also provide an approach for designing efficient regulatory tools in the future applications of type I CRISPR-Cas systems.

## RESULTS

### AcrIF11 Does Not Inactivate the CRISPR System by a Stable Direct Protein Interaction

First, we investigated the type I-F system-targeted Acrs whose inhibition mechanisms remain elusive. Because the structural basis of inhibition has already been revealed for AcrIF1/2/3/10 and AcrIF4 has already been shown to bind the Csy complex (Bondy-Denomy et al., 2015), we purified the remaining nine Acrs, mixed them with the purified 350-kDa Csy complex from *P. aeruginosa,* and performed a size-exclusion chromatography (SEC) assay. We intended to identify Acrs that co-elute with neither the Csy complex nor Cas2/3 and therefore might execute their inhibition with novel strategies. All tested Acrs, except AcrIF5, AcrIF11, and AcrIF12, co-eluted with the Csy complex, indicating a strong, direct, and stable protein interaction (Figures S1A–S1I). The lack of binding of the three remaining Acrs to the Csy complex led us to test whether they inhibit the CRISPR system by interacting with Cas2/3, as AcrIF3 does (Bondy-Denomy et al., 2015). However, they did not co-elute with the purified Cas2/3 (Figures S1J–S1M). Based on the lack of evidence for direct, stable protein interactions, we speculated that the three Acrs might have evolved strategies different from the known ones (AcrIF1/2/3/4/6/8/9/10) to inhibit the type I-F CRISPR system. This manuscript focuses on the inhibition mechanism of AcrIF11, whereas the detailed inhibition mechanism of AcrIF5 and AcrIF12 will be investigated in future studies.

### Crystal Structure of AcrIF11 Reveals that It Is a Novel mART

Because of the low sequence similarity of AcrIF11 with known domains, we determined its structure (full length, 132 residues) at 3.07 Å (Figure 1A; Table 1). The structure of AcrIF11 can be divided into two lobes, a β lobe composed of mainly a six-stranded β sheet (cyan) and an α-helical lobe spanning the residues from 51 to 107 (green, Figures 1A, S2A, and S2B). During the additive screen of the optimization steps, we found that the crystals of AcrIF11 required β-nicotinamide adenine dinucleotide (β-$NAD^+$, shortened to NAD hereafter) as an additive to show better diffraction. The final refined structure of AcrIF11 also showed a clear density for a NAD molecule located within the cleft formed on the surface of the β lobe (Figure 1A). Structural alignment using the DALI (distance-matrix alignment) server (Holm, 2019) did not reveal entries with *Z* scores higher than 7, but the catalytic domain (C domain) of diphtheria toxin (DT) (PDB: 1TOX) was found to be the closest structural homolog of AcrIF11, with a root-mean-square deviation (RMSD) of 3.1 Å among 92 residues. Although sequence alignment indicated that the two proteins display limited homology (Figure S2C), a superimposition of the three-dimensional structures of the C domain of DT and AcrIF11 revealed considerable structural similarities (Figure 1B). DT, an ~58-kDa protein secreted by *Corynebacterium diphtheriae*,

Please cite this article in press as: Niu et al., A Type I-F Anti-CRISPR Protein Inhibits the CRISPR-Cas Surveillance Complex by ADP-Ribosylation, Molecular Cell (2020), https://doi.org/10.1016/j.molcel.2020.09.015



CellPress

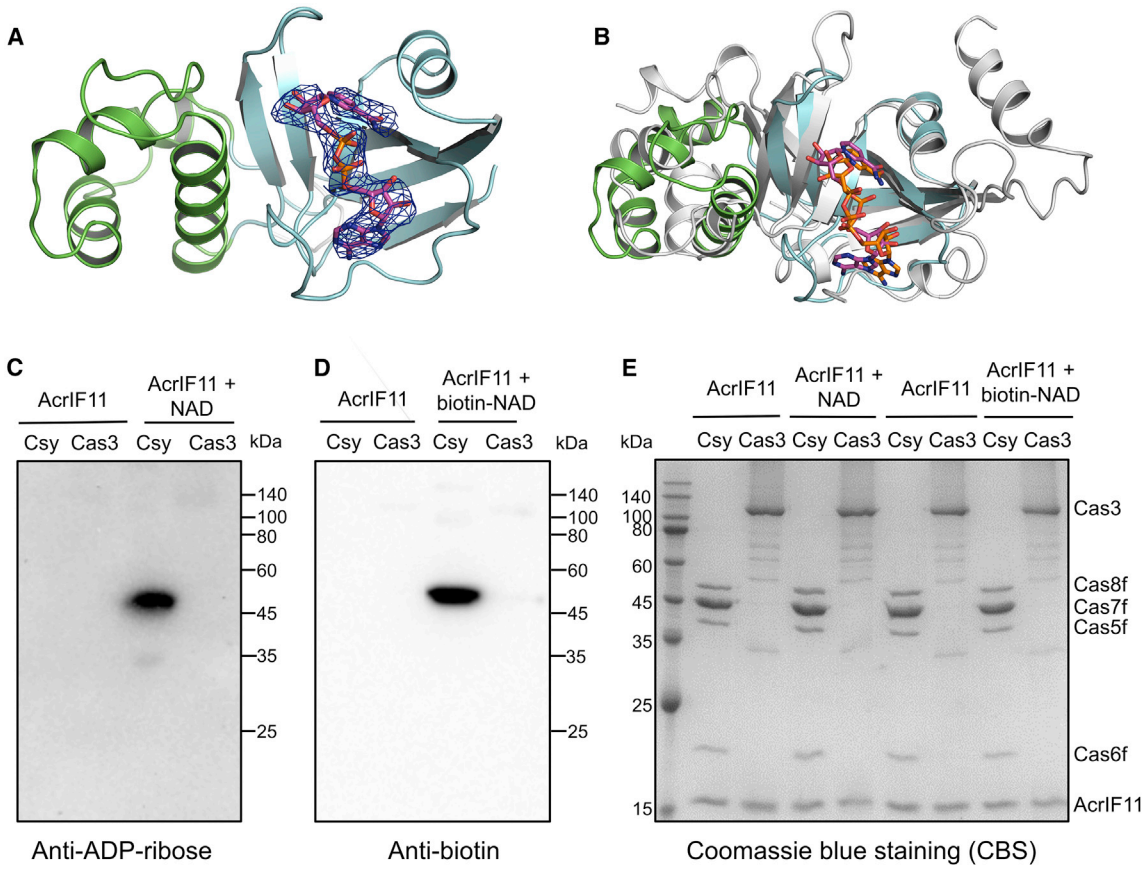



**Figure 1. AcrIF11 Is a Novel mART that Modifies the Csy Complex**

(A) Overall structure of AcrIF11. The α-helical and β lobes are colored in green and cyan, respectively. Shown in blue mesh is the simulated annealing composite omit map contoured at 3 σ around the NAD molecule in the stick model.

(B) Structural superimposition of AcrIF11 with the catalytic domain (C domain) of diphtheria toxin (DT) (PDB: 1TOX). AcrIF11 is colored as in (A). The C domain of DT is in gray, and the NAD molecule in the structure is shown as orange sticks.

(C and D) Csy complex or Cas2/3 was incubated with AcrIF11 in the presence or absence of NAD (C) or biotin-NAD (D). Then, the mixture was analyzed by SDS-PAGE and immuno-blotted with the polyclonal pan-ADP-ribose-recognizing antibody (C) or anti-biotin antibody (D), respectively. Cas3 indicates Cas2/3 in the type I-F CRISPR system.

(E) Same reaction mixtures in (C) and (D) were subjected to SDS-PAGE followed by Coomassie blue staining (CBS).

See also Figures S1 and S2 and Table 1.

causes the disease diphtheria in humans by inhibiting protein synthesis (Bell and Eisenberg, 1996). The C domain of DT possesses ADP-ribosylation activity, which uses NAD as a substrate to catalyze the covalent transfer of the ADP-ribose moiety from NAD to the diphthamide (post-translationally modified His715) of elongation factor-2 (EF-2) (Bell and Eisenberg, 1996). We therefore tested whether AcrIF11 would ADP-ribosylate proteins by performing an ADP-ribosylation assay using the Csy complex or Cas2/3 as a substrate and NAD or biotin-labeled NAD (biotin is attached to the amino group of the adenine base) as co-substrates. Immunoblotting using a polyclonal pan-ADP-ribose-recognizing antibody (anti-mono-ADP-ribose and poly-ADP-ribose, specifically detecting ADP-ribosylated proteins, for experiments with NAD as a substrate) and streptavidin blots (for experiments with biotin-NAD as a substrate) both clearly revealed that the Csy complex, but not Cas2/3, is ADP-ribosylated by AcrIF11 in the presence of NAD or biotin-NAD (Figures 1C–1E). The molecular weight of the modified band approximately corresponds to the Cas8f subunit (Figures 1C–1E). Altogether, these data revealed that AcrIF11 is an ADP-ribosyltransferase that modifies the Csy complex, probably at its Cas8f subunit.

## NAD Binding and Catalytic Mechanism of AcrIF11

AcrIF11 exhibits other distinct features apart from its low structural similarity with known ADP-ribosyltransferases. In the active site, the DT-like toxin family possesses a conserved HYE motif with a His residue, two Tyr residues, and a Glu residue (Figure S2D). The Glu residue, known as the key catalytic residue during the ADP-ribose transfer, is invariant even among all known bacterial ADP-ribosyltransferases (Simon et al., 2014). However, in AcrIF11, only the His residue is conserved (H7 in AcrIF11), but the two Tyr residues and the key Glu residue are replaced by F26, H37, and D115, respectively (Figures S2D–S2F). Next, we analyzed the binding mode of NAD within the AcrIF11

Please cite this article in press as: Niu et al., A Type I-F Anti-CRISPR Protein Inhibits the CRISPR-Cas Surveillance Complex by ADP-Ribosylation, Molecular Cell (2020), https://doi.org/10.1016/j.molcel.2020.09.015



**Table 1. Data Collection and Refinement Statistics**

| Data Collection | AcrIF11 (SeMet) |
|---|---|
| Space group | $P6_222$ |
| Cell Dimensions | |
| a, b, c (Å) | 104.677, 104.677, 119.673 |
| α, β, γ (°) | 90.00, 90.00, 120 |
| Resolution (Å) | 50–3.07 (3.21–3.07)[b] |
| $R_{sym}$ or $R_{merge}$ (%) | 14.5 (113.8) |
| I/σ(I) | 29.7 (2.8) |
| Completeness (%) | 99.5 (96.4) |
| Redundancy | 13.8 (13.0) |
| Refinement | |
| Resolution (Å) | 45.33–3.07 |
| No. reflections | 7640 |
| $R_{work}/R_{free}$[a] | 0.2046/0.2227 |
| No. atoms | 1090 |
| Protein | 1046 |
| Ligand/ion | 44 |
| Water | 0 |
| B factors | 79.43 |
| Protein | 79.23 |
| Ligand/ion | 84.22 |
| Water | |
| RMSDs | |
| Bond length (Å) | 0.003 |
| Bond angle (°) | 0.65 |
| Ramachandran Plot (%) | |
| Favored | 100 |
| Allowed | 0 |
| Outliers | 0 |

[a]For each structure, one crystal was used.
[b]Values in parentheses are for the highest-resolution shell.

structure. In the AcrIF11 structure, NAD forms a ring-like conformation in the cavity within the β lobe (Figure 2A). The nicotinamide group is stabilized by two hydrogen bonds from the carbonyl oxygen and amide nitrogen of G8 and π-π interaction with the side chain of H37 (Figure 2A). Moreover, the adenine group is stabilized by the polar interaction from the carbonyl oxygen of R17, and the ribose moiety within the ADP part is hydrogen bonded to the side chains of H7, S9, and E11. In addition, the NAD molecule is bound by hydrophobic interactions by the side chains of F26 and H117 (Figure 2A). Notably, NAD was indispensable for the inhibition of the type I-F CRISPR DNA strand cleavage *in vitro* by AcrIF11 (Figure 2B, lanes 4 and 5). Moreover, mutations of the NAD binding residues of AcrIF11 abolished both its ADP-ribosylation activity (Figure 2C) and its capacity of inhibiting DNA cleavage *in vitro* (Figure 2B). The decreased binding to NAD by the AcrIF11 mutants was confirmed using the isothermal titration calorimetry (ITC) assay (Figures 2D and S3A–S3I). A single mutation of D115 did not completely inhibit NAD binding but was enough to abolish the ADP-ribosylation of the Csy complex, suggesting that this residue is essential during the catalytic process. This is in agreement with the core catalytic Glu residue, which shares the similar spatial position in known bacterial ADP-ribosyltransferases (Figure S2F). Deletion of the α-helical lobe also caused loss of modification activity of AcrIF11, suggesting that the α-helical lobe is integral to the structure of AcrIF11 (Figure S4A). AcrIF11 was not able to deplete the NAD pool in the host cell (Figures S4B and S4C). Collectively, these data suggested that the ADP-ribosylation activity of AcrIF11 is essential for inhibiting the type I-F CRISPR system.

## AcrIF11 Inhibits the Csy Complex through ADP-Ribosylation of the PAM-Recognition Residue N250 of Cas8f

Next, we aimed to elucidate how ADP-ribosylation would inhibit the activity of the Csy complex. First, we mapped the modification sites of the AcrIF11-modified subunit of the Csy complex. We co-expressed the Csy complex with AcrIF11, purified the Csy complex, and separated the purified complex via SDS-PAGE. Immunoblotting with the anti-ADP-ribose antibody revealed that the band corresponding to the Cas8f subunit of the Csy complex was modified by AcrIF11, whereas this was not the case when the Csy complex was expressed and analyzed alone (Figure 3A). Upon tryptic digestion, liquid chromatography-mass spectrometry (LC-MS) detected a peptide sequence, $F_{243}$GGTKPQNISQLNSER$_{258}$, of Cas8f with a mass addition of 541 Da, consistent with the attachment of the ADP-ribose moiety. Further tandem mass spectrometry by electron transfer dissociation (ETD) unambiguously mapped the site of ADP-ribosylation to N250 of Cas8f (Figures 3B and S5A; Tables S1 and S2). Because of the similar size between Cas8f and Cas7f, we also performed mass spectrometry analysis of the Cas7f subunit, which did not reveal strong evidence supporting potential modification of detected peptide sequences (Table S3). N250 of Cas8f has been identified as a key residue for PAM recognition (Rollins et al., 2019), forming hydrogen bonding interactions with $dG^{-1}$ (Figure 3C). Consistently, mutation of N250 of Cas8f substantially reduced the double-stranded DNA (dsDNA) binding activity of the Csy complex in an EMSA (electrophoretic mobility shift assay) experiment (Figure 3D). We thus verified the ADP-ribosylation site by mutagenesis of N250. Replacement of N250 with different residues abolished the modification of Cas8f by AcrIF11 (Figure 3E). K247 of Cas8f, a residue adjacent to N250, was also suggested to be involved in target DNA binding by previous studies (Guo et al., 2017; Rollins et al., 2019). Although the K247A mutation did not cause an obvious defect in dsDNA binding under our experimental conditions, the K247E mutation severely decreased the binding in the same assay (Figure 3D), which is consistent with the results of a recent study (Rollins et al., 2019). Interestingly, we found that mutation of K247 also dampens Cas8f modification by AcrIF11 (Figure 3E), suggesting that $Cas8f^{K247}$ may be involved in the binding of AcrIF11. To test this possibility, we performed ITC binding assays, which confirmed that mutation of N250 or K247 of Cas8f markedly decreases or even abolishes the binding of AcrIF11 to the Csy complex, respectively (Figures 3F and S3J–S3N). In all, AcrIF11 catalyzes the ADP-ribosylation of N250 of the Cas8f subunit within the Csy complex (Figure 3G).

Please cite this article in press as: Niu et al., A Type I-F Anti-CRISPR Protein Inhibits the CRISPR-Cas Surveillance Complex by ADP-Ribosylation, Molecular Cell (2020), https://doi.org/10.1016/j.molcel.2020.09.015



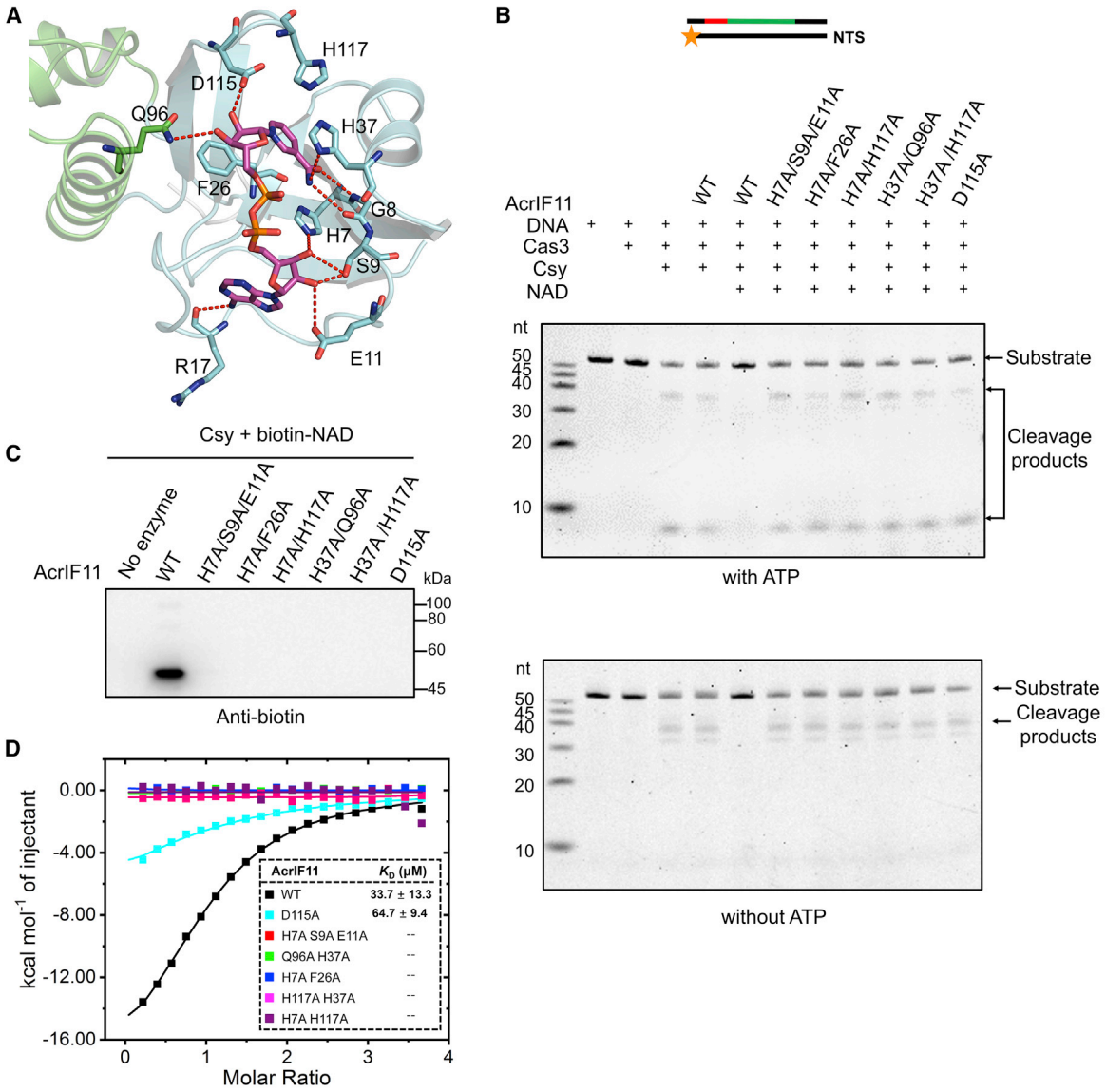



**Figure 2. The Catalytic and NAD Binding Residues of AcrIF11 Are Important for Both ADP-Ribosylation and Inhibition**

(A) Binding details of NAD in AcrIF11. The structure of AcrIF11 is shown as in Figure 1A, and the residues involved in NAD binding are shown as sticks. Hydrogen bonds are shown as red dashed lines.

(B) Mutations of the catalytic and NAD binding residues of AcrIF11 decreased its capacity of inhibition of the *in vitro* cleavage activity toward the type I-F CRISPR system. Reactions were performed with 0.8 μM Csy complex and 40 nM 54-bp dsDNA (5′-FAM in the non-target DNA strand, NTS). AcrIF11 or its mutants, Cas2/3, and NAD were added with a concentration of 2.4, 0.4, and 25 μM, respectively, when needed. The red and green lines indicate PAM and the protospacer region, respectively, which are used throughout the study.

(C) Mutations of the catalytic and NAD binding residues of AcrIF11 decreased its ADP-ribosylating activity. The Csy complex was incubated with AcrIF11 or its mutants, and then the samples were treated as in Figure 1D.

(D) Isothermal titration calorimetry (ITC) assays to test binding of AcrIF11 and its mutants to NAD. Representative binding curves are shown. $K_D$ values are mean ± SEM (n = 2). Raw data for these curves are shown in Figures S3A–S3I.

See also Figures S2–S4 and Table 1.

## ADP-Ribosylation of N250 of Cas8f Prevents Binding of Csy to Its Target DNA

Based on the Csy-dsDNA complex structure, ADP-ribosylation of N250 may not only eliminate the hydrogen bonding interactions with $dG^{-1}$ but also sterically hinder the interaction with neighboring PAM DNA because of the bulky ADP-ribose moiety (Figure 3C), thus preventing the Csy complex from binding to dsDNA. To test this, we performed EMSAs to study the Csy-dsDNA interaction in the presence of AcrIF11 or AcrIF11/NAD. Although AcrIF11 alone did not cause a marked decrease in

Please cite this article in press as: Niu et al., A Type I-F Anti-CRISPR Protein Inhibits the CRISPR-Cas Surveillance Complex by ADP-Ribosylation, Molecular Cell (2020), https://doi.org/10.1016/j.molcel.2020.09.015



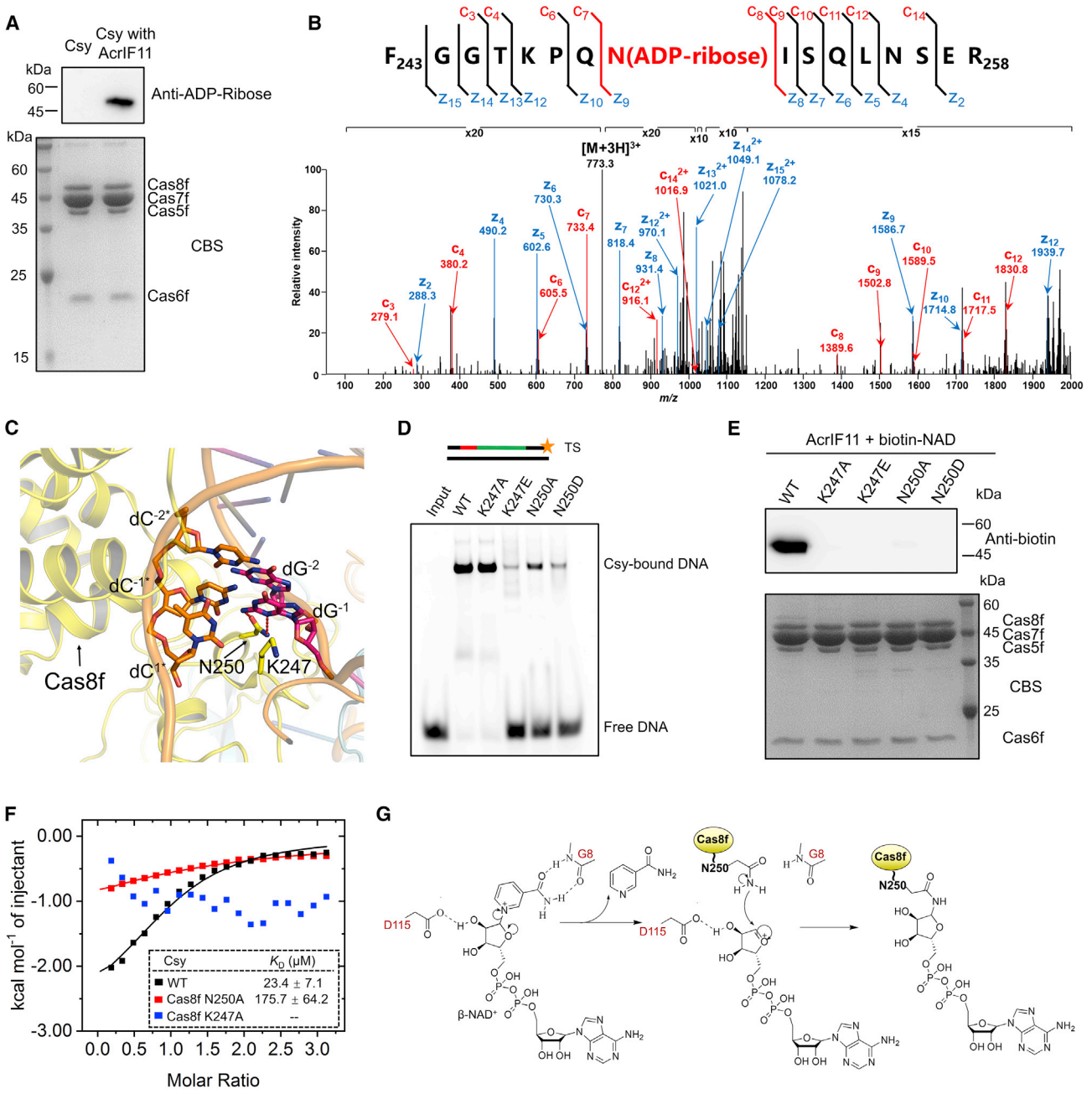



**Figure 3. AcrIF11 Inhibits the Csy Complex through ADP-Ribosylation of the PAM-Recognition Residue N250 of Cas8f**

(A) Csy complex expressed alone or with AcrIF11 were purified, subjected to SDS-PAGE and immune-blotted with the polyclonal pan-ADP-ribose-recognizing antibody, or stained by CBS.

(B) Tandem mass spectrometry (MS/MS) spectrum of ADP-ribosylated $F_{243}$GGTKPQNISQLNSER$_{258}$ by ETD analysis. $c_8$ and $z_9$ fragment ions indicate that the modification site is located at N250 of Cas8f of the Csy complex.

(C) Magnification of the PAM interaction details in the structure of the dsDNA-bound Csy complex (PDB: 6NE0). The Cas8f subunit of the Csy complex is in yellow.

(D) EMSA used to test the dsDNA binding activity of Csy and its mutants of the Cas8f subunit. Reactions were performed with 8 μM Csy complex or its Cas8f mutants and 0.5 μM 54-bp dsDNA (5′-FAM in the target DNA strand, TS).

(E) Csy complex or its mutants of the Cas8f subunit were incubated with AcrIF11 and biotin-NAD, and then the samples were treated as in Figure 1D. The Csy complex or its mutants were also visualized by CBS (lower panel).

*(legend continued on next page)*

Please cite this article in press as: Niu et al., A Type I-F Anti-CRISPR Protein Inhibits the CRISPR-Cas Surveillance Complex by ADP-Ribosylation, Molecular Cell (2020), https://doi.org/10.1016/j.molcel.2020.09.015



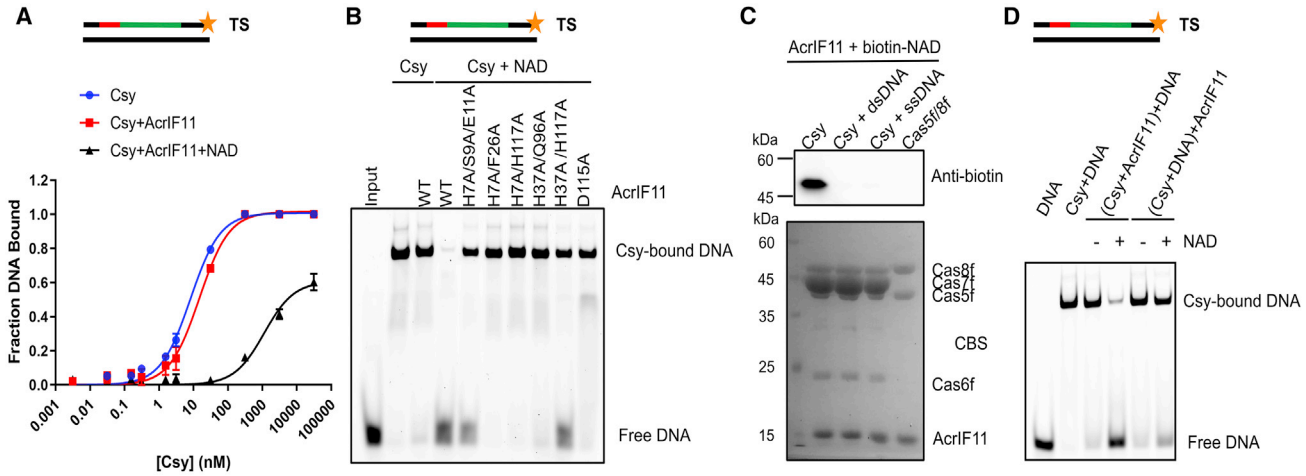



**Figure 4. AcrIF11-Mediated ADP-Ribosylation of the Csy Complex Prevents Target DNA Binding**

(A) EMSA performed with dsDNA substrates shows that incubation with AcrIF11/NAD results in reduced crRNA-guided DNA binding. Error bars represent SEM; n = 3. The $K_D$ values are 8.18 ± 0.82, 14.87 ± 2.32, and 1,136 ± 253.8 nM for Csy, Csy with AcrIF11, and Csy with AcrIF11/NAD, respectively. Raw data for these curves are shown in Figure S6.

(B) EMSA used to test the dsDNA binding activity of the Csy complex in the presence of AcrIF11 or its NAD-binding-deficient mutants. Reactions were performed with 8 μM Csy complex and 0.5 μM 54-bp dsDNA (5′-FAM in the TS). AcrIF11 or its mutants and NAD were added with a concentration of 32 and 50 μM, respectively, when needed.

(C) AcrIF11 and biotin-NAD were incubated with the Csy complex, dsDNA-bound Csy complex, complimentary ssDNA-bound Csy complex, and Cas5f/8f subcomplex. Then, the samples were treated as in Figure 3E.

(D) EMSA used to test the effect of dsDNA binding on the inhibition capacity of AcrIF11. AcrIF11 was added to the Csy complex before or after adding dsDNA, in the presence or absence of NAD. The concentrations of the Csy complex, 54-bp dsDNA, AcrIF11, and NAD were the same as in (B). Preformed complexes are shown in parentheses.

See also Figure S6.

Csy-dsDNA binding, incubation with AcrIF11/NAD severely decreased Csy-dsDNA binding (Figures 4A and S6), similar to the situation with inhibition of *in vitro* DNA cleavage by AcrIF11 (Figure 2B, lanes 4 and 5). Consistently, our biochemical data demonstrated that only wild type, but not the NAD-binding-deficient mutants of AcrIF11, could substantially reduce the dsDNA binding activity of the Csy complex in the presence of NAD (Figure 4B). This clearly indicates that AcrIF11 affects the Csy complex with a different mechanism compared with the other known AcrIF proteins and even other Acrs (Bondy-Denomy et al., 2015; Zhang et al., 2020). Our biochemical and structural data showed that AcrIF11 inhibits the type I-F CRISPR system through ADP-ribosylation of the critical PAM-interacting residue N250 of the Cas8f subunit of the Csy complex, thus preventing binding to the dsDNA target. The Csy-dsDNA structure also indicates that both the K247 and the N250 sites of Cas8f will be protected from recognition by AcrIF11 in the dsDNA-bound form of the Csy complex (Figure 3C). This was confirmed by the strongly decreased ADP-ribosylation of the dsDNA-saturated Csy complex by AcrIF11 *in vitro* (Figure 4C). EMSA also suggested that preincubation of the Csy complex with dsDNA substantially reduced the inhibitory effect of AcrIF11 (Figure 4D). Preincubation of the Csy complex with complimentary single-stranded DNA (ssDNA) also inhibits N250 modification, indicating that the binding site of ssDNA might partially overlap that of AcrIF11 (Figure 4C).

## AcrIF11 Carries Out Its Modification Only in the Context of the Csy Complex by Recognizing Cas7f

Next, we tested whether AcrIF11 could modify the Cas8f subunit in the form of the Cas5f-Cas8f subcomplex alone, because these two subunits could form a stable complex (Hong et al., 2018). AcrIF11 only ADP-ribosylated the Cas8f subunit in the context of the whole Csy complex, but not the Cas5f-Cas8f subcomplex (Figure 4C). This suggested that other parts of the Csy complex, i.e., the Cas7f and/or Cas6f subunits, would facilitate the modification of Cas8f by AcrIF11. Considering the molecular size of AcrIF11, we speculated that the Cas7f subunits adjacent to Cas8f might interact with AcrIF11. Electrostatic analysis of the structure of AcrIF11 indicated that it has several negatively charged surfaces (Figure 5A), consistent with it overlapping the PAM region of the targeting DNA. Therefore, several surface regions, mostly positively charged, of the Cas7f subunits of the Csy complex were mutagenized (Figure 5B), and these mutants

(F) ITC assays to test binding of Csy and its mutants to AcrIF11. Representative binding curves are shown for Csy and its Cas8f$^{N250A}$ mutant. Binding could not be detected for the Csy Cas8f$^{K247A}$ mutant, and the data were not fitted. $K_D$s are mean ± SEM (n = 2). Raw data for these curves are shown in Figures S3J–S3N.

(G) Proposed structure-based mechanism for ADP-ribosylation of the Cas8f subunit of the Csy complex. The reaction was proposed to proceed in an SN1-like mechanism (Cohen and Chang, 2018; Han et al., 2001). The AcrIF11 residues involved in the catalytic reaction are marked in red.

See also Figures S3, S5, and S7 and Tables S1, S2, and S3.

Please cite this article in press as: Niu et al., A Type I-F Anti-CRISPR Protein Inhibits the CRISPR-Cas Surveillance Complex by ADP-Ribosylation, Molecular Cell (2020), https://doi.org/10.1016/j.molcel.2020.09.015



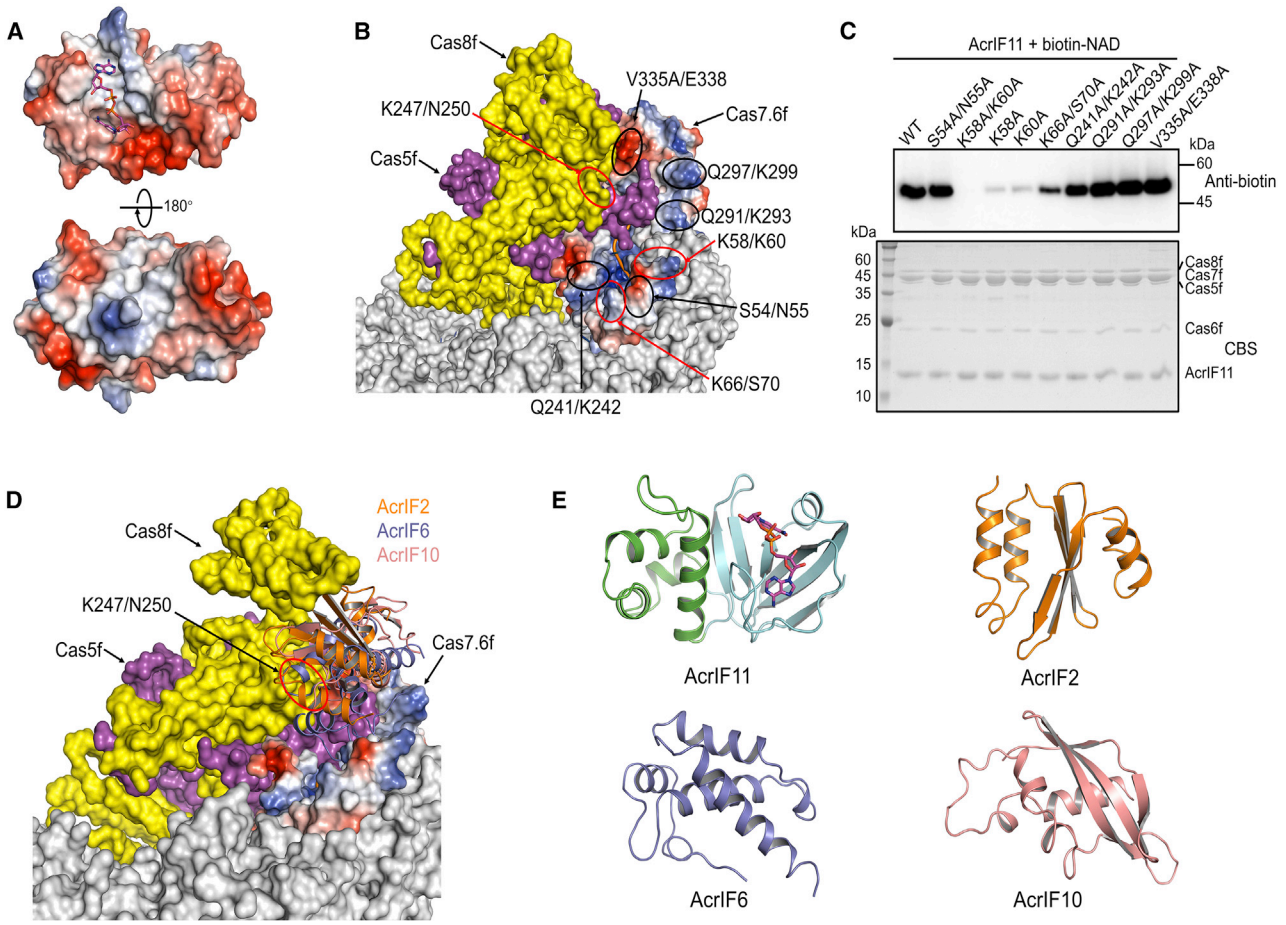



**Figure 5. AcrIF11 Requires the Cas7f Subunit of the Csy Complex to Carry Out Its Modification**

(A) Electrostatic surface model of AcrIF11 is shown in two angles. NAD is shown in sticks.

(B) Surface model of the Csy complex (PDB: 6B45). The Cas8f, Cas5f, and Cas7.6f subunits of the Csy complex are shown in yellow, magenta, and electrostatic mode, respectively. Patches selected for mutation are highlighted in circles. The patches of residues, whose mutations decrease or abolish the modification by AcrIF11, are marked with red circles, and the others are in black circles.

(C) Csy complex or its mutants of the Cas7f subunit were incubated with AcrIF11 and biotin-NAD, and then the samples were treated as in Figure 3E.

(D) K247/N250 patch is engaged by AcrIF2/6/10. Surface model of the Csy complex (PDB: 6B45). The Cas8f, Cas5f, and Cas7.6f subunits of the Csy complex are shown as in (B). The structures of Csy-AcrIF2 (PDB: 6B47), Csy-AcrIF6 (PDB: 6VQX), and Csy-AcrIF10 (PDB: 6B48) are aligned to that of the Csy complex, and AcrIF2/6/10 is shown in the cartoon model. The K247/N250 patch is marked with a red circle.

(E) Overall structures of AcrIF11 and AcrIF2/6/10. Cartoon models of AcrIF11 and AcrIF2/6/10. AcrIF11 is colored as in Figure 1A.

See also Figures S3 and S7.

were subsequently tested for whether they could affect the ADP-ribosylation of the Csy complex by AcrIF11 (Figure 5C). Interestingly, among the tested mutants, the K58A/K60A mutation of Cas7f rendered the Csy complex resistant to ADP-ribosylation by AcrIF11, and single mutation of K58 or K60 markedly decreased this modification (Figure 5C). Moreover, mutations of K66A/S70A partially weakened the ADP-ribosylation of the Csy complex by AcrIF11 (Figure 5C). This suggested that these regions of Cas7f might also be important for the binding of the Csy complex by AcrIF11. A further ITC assay confirmed that single mutation of K58A and K60A of Cas7f also abolishes the interaction between the Csy complex and AcrIF11 (Figures S3O and S3P). The Cas7f$^{K66A/S70A}$ mutant of Csy only exhibits slightly decreased binding to AcrIF11 (Figures S3Q and S3R), indicating that other structural constraints might explain the defective ADP-ribosylation for this mutant. Altogether, besides Cas8f, Cas7f is indispensable for both binding to and modification of the Csy complex by AcrIF11.

## DISCUSSION

ADP-ribosylation, as a widespread protein post-translational modification, has been linked to many cellular processes, including different forms of stress responses and metabolism (Hopp et al., 2019; Qi et al., 2019). Our study reveals, for the first time to our knowledge, that ADP-ribosylation is used by Acr proteins to inactivate the CRISPR adaptive immune system. AcrIF11 interacts with the PAM-recognition residues Cas8f$^{K247}$ (primarily)

Please cite this article in press as: Niu et al., A Type I-F Anti-CRISPR Protein Inhibits the CRISPR-Cas Surveillance Complex by ADP-Ribosylation, Molecular Cell (2020), https://doi.org/10.1016/j.molcel.2020.09.015





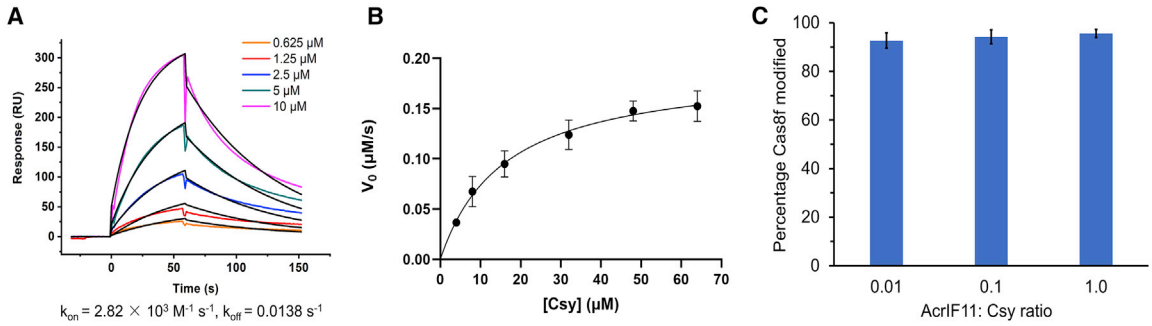



**Figure 6. Binding Kinetics and Enzymatic Activity of AcrIF11**

(A) Binding kinetics of AcrIF11 with the Csy complex, measured by SPR. SPR curves (colored curves) were fit kinetically using a 1:1 Langmuir binding model (black lines). Data shown are representative of three independent experiments.

(B) Kinetic analysis of AcrIF11 showing dependence of initial velocity on the concentration of the Csy complex. Measurements were obtained using 300 μM ε-NAD and 0.5 μM AcrIF11 at 25°C and fit to a standard Michaelis-Menten model using GraphPad Prism software. The calculated $K_m$ for the Csy complex and $k_{cat}$ are 15.98 μM and 0.383 $s^{-1}$, respectively. Data shown are mean ± SD (n = 3 independent experiments).

(C) AcrIF11 is a multiple-turnover enzyme for ADP-ribosylation of the Cas8f subunit. Percentage of the modified Cas8f subunit after 1 h at different molar ratios of AcrIF11 to the Csy complex (mean ± SD, n = 3 independent experiments). The representative results of liquid chromatography-tandem mass spectrometry (LC-MS/MS) used to calculate the modification percentage are shown in Figure S5B.

See also Figure S5.

and $Cas8f^{N250}$ of the Csy complex and ADP-ribosylates $Cas8f^{N250}$. These two residues, together with the residues within the K247/N250-containing loop (the K wedge) (Guo et al., 2017), are highly conserved among Cas8f homologs (Figure S7). In addition, the K58/K60 patch of Cas7f is essential for the binding of AcrIF11. Based on the structure of the Csy complex and the molecular size of AcrIF11, Cas7.6f, the Cas7f subunit adjacent to the Cas5f/8f subcomplex, is the most likely Cas7f subunit to participate in AcrIF11 interaction. AcrIF2, AcrIF10, and most recently AcrIF6 were also found to bind at the junction between Cas7.6f and Cas8f (Chowdhury et al., 2017; Guo et al., 2017; Peng et al., 2017; Zhang et al., 2020). Moreover, the K247/N250 patch of Cas8f is engaged by all of these Acr proteins to prevent PAM recognition, as observed by the structures of Csy complexed with each Acr protein (Figure 5D). AcrIF11 did not share structural similarities to AcrIF2/6/10 (Figure 5E). Despite extensive trials, we have failed so far to obtain a stable AcrIF11-Csy complex to structurally characterize the detailed interaction mode between them due to the low binding affinity.

The $K_D$ value between AcrIF11 and the Csy complex was weaker than those observed for other Acr proteins, such as AcrIF1, with 2.5 × $10^{-11}$ M (Chowdhury et al., 2017), and AcrIF4, with 4 × $10^{-7}$ M (Borges et al., 2018). This explains why the binding between AcrIF11 and the Csy complex cannot be observed through gel filtration. To investigate the detailed binding and catalytic parameters of AcrIF11, we performed surface plasmon resonance (SPR) assays, which showed that $k_{on}$ and $k_{off}$ were 2.82 × $10^3$ $M^{-1}$ $s^{-1}$ and 0.0138 $s^{-1}$, respectively (Figure 6A). The binding $K_D$ calculated from this approach was 4.89 μM, slightly lower than that obtained through ITC (~23.4 μM), which is probably caused by the different principles of these two approaches. Moreover, enzymatic kinetics assay of AcrIF11 using 1, $N^6$-Etheno NAD (ε-NAD) as a co-substrate revealed that $K_m$ for the Csy complex and $k_{cat}$ were 15.98 μM and 0.383 $s^{-1}$, respectively (Figure 6B). $k_{cat}/K_m$ of AcrIF11 is 2.4 × $10^4$ $M^{-1}$ $s^{-1}$ and is close to an average enzyme (Bar-Even et al., 2011) based on the kinetic parameters. Moreover, we did not detect other ADP-ribosylation peaks in the mass spectrometry studies, suggesting that the enzymatic activity of AcrIF11 is highly specific under our experimental conditions.

Although AcrIF2/6/10 inactivates the type I-F CRISPR system through direct binding to the Csy complex to sterically block DNA recognition, AcrIF11 inhibits the system by enzymatic ADP-ribosylation of the essential PAM-recognition residue $Cas8f^{N250}$ of the Csy complex. To test whether AcrIF11 is a multiple-turnover inhibitor, we incubated AcrIF11 of three concentrations with a fixed concentration of the Csy complex and in all cases observed that more than 90% of the Csy complex was modified, even at sub-stoichiometric concentrations of AcrIF11 (Figures 6C and S5B). Enzymatic activity also makes AcrIF11 a more potent inhibitor than the other three Acr proteins. Consistently, AcrIF11 was able to fully inhibit both dsDNA binding by the Csy complex (Figure 7A) and *in vitro* DNA cleavage (Figure 7B) with a concentration 100 times lower than that of the other three Acrs under our experimental conditions.

Homologs of AcrIF11 were found in more than 50 species of diverse Proteobacteria (Marino et al., 2018), suggesting that this mode of inhibition might be widely used. Interestingly, only a portion of AcrIF11 homologs are associated with the type I-F CRISPR system (Table S4) (Zhang et al., 2018), and all of these associated type I-F systems share a similar PAM-recognition loop sequence in Cas8f (Figure S7). Some AcrIF11 homologs are exclusively associated with other types of the CRISPR system, such as types I-E, I-A, and IV-A (Table S4). We speculate that these AcrIF11 homologs may also mediate inhibition of other types of CRISPR-Cas systems. Future studies might identify novel substrates of AcrIF11 homologs.

Recently, AcrVA5 was found to inactivate the type V CRISPR-Cas12a (Cpf1) system through acetylation of the Cas12a protein (Dong et al., 2019), and AcrVA1 was able to cleave the

Please cite this article in press as: Niu et al., A Type I-F Anti-CRISPR Protein Inhibits the CRISPR-Cas Surveillance Complex by ADP-Ribosylation, Molecular Cell (2020), https://doi.org/10.1016/j.molcel.2020.09.015



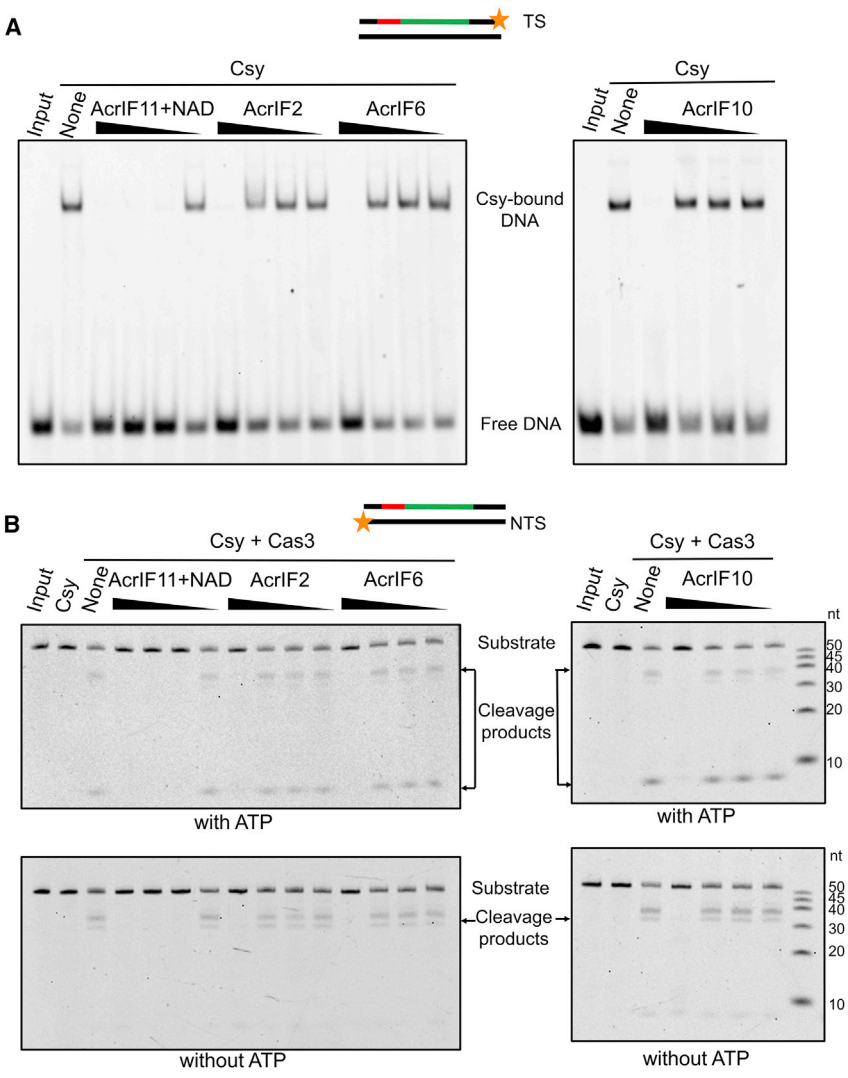



**Figure 7. AcrIF11 Is a More Potent Acr than AcrIF2/6/10**

EMSA (A) and *in vitro* DNA cleavage assay (B) were used to compare the inhibition capacity of AcrIF2/6/10/11 against a type I CRISPR-Cas system. For EMSA, reactions were performed with 1.6 μM Csy complex and 0.1 μM 54-bp dsDNA (5′-FAM in the TS) and Acrs concentrations of 4.8 μM, 0.48 μM, 48 nM, and 4.8 nM, following the order indicated by the black triangles. NAD was added with a concentration of 50 μM when needed. For the *in vitro* DNA cleavage assay, reactions were performed with 0.8 μM Csy complex, 0.04 μM 54-bp-dsDNA (5′-FAM in the NTS), 0.4 μM Cas3 and Acrs concentration of 2.4 μM, 0.24 μM, 24 nM, and 2.4 nM, following the order indicated by the black triangles. NAD was added with a concentration of 25 μM when needed.

See also Table S4.

target-recognition sequence of the Cas12a-bound crRNA, also inactivating the Cas12a complex (Knott et al., 2019; Zhang et al., 2019a). Covalent modifications of the CRISPR proteins by Acr proteins could more potently, and might permanently, inactivate the system and thus probably become a more efficient strategy to inhibit the CRISPR adaptive immune system. Another fascinating, yet unknown question is whether any species of bacteria might harbor eraser enzymes (O'Sullivan et al., 2019) to reverse the ADP-ribosylation introduced by AcrIF11. Further studies into this might uncover novel mechanisms and provide further insights into the competition between viral parasites and immune systems of their hosts.

Phages have evolved diverse mechanisms to inhibit CRISPR-Cas adaptive immune systems. Future studies to identify novel mechanisms will not only contribute to our understanding of the evolutionary arms race between phages and bacteria but also provide more strategies to engineer more efficient CRISPR-Cas systems or design regulatory tools in the applications of CRISPR-Cas systems.

## STAR★METHODS

Detailed methods are provided in the online version of this paper and include the following:

- KEY RESOURCES TABLE
- RESOURCE AVAILABILITY
  - Lead Contact
  - Materials Availability
  - Data and Code Availability
- EXPERIMENTAL MODEL AND SUBJECT DETAILS
- METHOD DETAILS
  - Protein expression and purification
  - Crystallization, data collection and structure determination
  - In vitro DNA cleavage assay
  - Gel filtration assay
  - Electrophoretic mobility shift assay
  - In-gel protein digestion and LC-MS/MS analyses

Please cite this article in press as: Niu et al., A Type I-F Anti-CRISPR Protein Inhibits the CRISPR-Cas Surveillance Complex by ADP-Ribosylation, Molecular Cell (2020), https://doi.org/10.1016/j.molcel.2020.09.015






- In vitro modification assay
- Isothermal titration calorimetry binding assay
- Enzymatic kinetics assay of AcrIF11
- Expression of AcrIF11 in Pseudomonas aeruginosa PA14 and $NAD^+$ quantification
- Surface Plasmon Resonance binding assay
- Analysis of AcrIF11-associated CRISPR systems

● QUANTIFICATION AND STATISTICAL ANALYSIS


## SUPPLEMENTAL INFORMATION

Supplemental Information can be found online at https://doi.org/10.1016/j.molcel.2020.09.015.

## ACKNOWLEDGMENTS

We thank Prof. Zhiwei Huang for discussions of the bioinformatics results of AcrIF11, Prof. Weihui Wu for the gift of the *Pseudomonas aeruginosa* PA14 strain and the pUCP19 vector, and Dr. Song Xue for discussions of the enzymatic kinetics assays. We thank the staff at beamlines BL17U1 and BL19U1 of the Shanghai Synchrotron Radiation Facility for their assistance with data collection. We thank Dr. Wei Zhang of the Institute of Microbiology, CAS, for assisting with the SPR experiments. We thank the Tsinghua University Branch of China National Center for Protein Sciences Beijing and Shilong Fan for providing facility support for X-ray diffraction of the crystal samples. We acknowledge the Protein Preparation and Characterization Core Facility of Tsinghua University Branch of China National Center for Protein Sciences Beijing for providing facility support. This work was supported by the National Natural Science Foundation of China (31822012 and 21974002), the National Key Research and Development Program of China (2017YFA0506500, 2017YFD0500305, 2017YFD0500901, and 2019YFC1200502), the State Key Program of National Natural Science of China (U1808202), the Beijing Nova program, and Fundamental Research Funds for the Central Universities (XK1802-8).

## AUTHOR CONTRIBUTIONS

Y.F. conceived and supervised the project. Y.N., L.Y., T.G., C.D., P.Y., Xi Liu, X.C., and Y.X. purified the proteins, grew and optimized the crystals, collected the diffraction data, and performed most *in vitro* activity analysis and binding assays, supervised by Y.Z. and Z.C. Y.F. and Y.Z. solved the structure. B.Z. and H.W. identified the modification site of Cas8f and conducted other mass spectrometry studies, supervised by Xiaoyun Liu. A.-K.H. and M.O.H. provided the anti-mono-ADP-ribose antibody and technical support. D.L. performed part of the binding assays. R.G. conducted bioinformatics analysis. X.M., H.D., and X.Z. contributed to the mass spectrometry analysis. J.R. made the reaction scheme and contributed to the enzymatic kinetics assays. Y.F. and Y.Z. analyzed the data and wrote the original manuscript. Y.F., M.O.H., A.-K.H., and Xiaoyun Liu revised the paper with assistance from all authors.

## DECLARATION OF INTERESTS

The authors declare no competing interests.

Received: April 29, 2020
Revised: August 11, 2020
Accepted: September 11, 2020
Published: October 12, 2020

## REFERENCES

Adams, P.D., Grosse-Kunstleve, R.W., Hung, L.W., Ioerger, T.R., McCoy, A.J., Moriarty, N.W., Read, R.J., Sacchettini, J.C., Sauter, N.K., and Terwilliger, T.C. (2002). PHENIX: building new software for automated crystallographic structure determination. Acta Crystallogr. D Biol. Crystallogr. *58*, 1948–1954.

Athukoralage, J.S., McMahon, S.A., Zhang, C., Grüschow, S., Graham, S., Krupovic, M., Whitaker, R.J., Gloster, T.M., and White, M.F. (2020). An anti-CRISPR viral ring nuclease subverts type III CRISPR immunity. Nature *577*, 572–575.

Bar-Even, A., Noor, E., Savir, Y., Liebermeister, W., Davidi, D., Tawfik, D.S., and Milo, R. (2011). The moderately efficient enzyme: evolutionary and physicochemical trends shaping enzyme parameters. Biochemistry *50*, 4402–4410.

Bell, C.E., and Eisenberg, D. (1996). Crystal structure of diphtheria toxin bound to nicotinamide adenine dinucleotide. Biochemistry *35*, 1137–1149.

Bhoobalan-Chitty, Y., Johansen, T.B., Di Cianni, N., and Peng, X. (2019). Inhibition of Type III CRISPR-Cas Immunity by an Archaeal Virus-Encoded Anti-CRISPR Protein. Cell *179*, 448–458.

Bondy-Denomy, J., Pawluk, A., Maxwell, K.L., and Davidson, A.R. (2013). Bacteriophage genes that inactivate the CRISPR/Cas bacterial immune system. Nature *493*, 429–432.

Bondy-Denomy, J., Garcia, B., Strum, S., Du, M., Rollins, M.F., Hidalgo-Reyes, Y., Wiedenheft, B., Maxwell, K.L., and Davidson, A.R. (2015). Multiple mechanisms for CRISPR-Cas inhibition by anti-CRISPR proteins. Nature *526*, 136–139.

Borges, A.L., Zhang, J.Y., Rollins, M.F., Osuna, B.A., Wiedenheft, B., and Bondy-Denomy, J. (2018). Bacteriophage Cooperation Suppresses CRISPR-Cas3 and Cas9 Immunity. Cell *174*, 917–925.

Choi, K.H., Kumar, A., and Schweizer, H.P. (2006). A 10-min method for preparation of highly electrocompetent Pseudomonas aeruginosa cells: application for DNA fragment transfer between chromosomes and plasmid transformation. J. Microbiol. Methods *64*, 391–397.

Chowdhury, S., Carter, J., Rollins, M.F., Golden, S.M., Jackson, R.N., Hoffmann, C., Nosaka, L., Bondy-Denomy, J., Maxwell, K.L., Davidson, A.R., et al. (2017). Structure Reveals Mechanisms of Viral Suppressors that Intercept a CRISPR RNA-Guided Surveillance Complex. Cell *169*, 47–57.e11.

Cohen, M.S., and Chang, P. (2018). Insights into the biogenesis, function, and regulation of ADP-ribosylation. Nat. Chem. Biol. *14*, 236–243.

Dolan, A.E., Hou, Z., Xiao, Y., Gramelspacher, M.J., Heo, J., Howden, S.E., Freddolino, P.L., Ke, A., and Zhang, Y. (2019). Introducing a Spectrum of Long-Range Genomic Deletions in Human Embryonic Stem Cells Using Type I CRISPR-Cas. Mol. Cell *74*, 936–950.e5.

Dong, L., Guan, X., Li, N., Zhang, F., Zhu, Y., Ren, K., Yu, L., Zhou, F., Han, Z., Gao, N., and Huang, Z. (2019). An anti-CRISPR protein disables type V Cas12a by acetylation. Nat. Struct. Mol. Biol. *26*, 308–314.

Eitzinger, S., Asif, A., Watters, K.E., Iavarone, A.T., Knott, G.J., Doudna, J.A., and Minhas, F.U.A.A. (2020). Machine learning predicts new anti-CRISPR proteins. Nucleic Acids Res. *48*, 4698–4708.

Emsley, P., Lohkamp, B., Scott, W.G., and Cowtan, K. (2010). Features and development of Coot. Acta Crystallogr. D Biol. Crystallogr. *66*, 486–501.

Forsberg, K.J., Bhatt, I.V., Schmidtke, D.T., Javanmardi, K., Dillard, K.E., Stoddard, B.L., Finkelstein, I.J., Kaiser, B.K., and Malik, H.S. (2019). Functional metagenomics-guided discovery of potent Cas9 inhibitors in the human microbiome. eLife *8*, e46540.

Guo, T.W., Bartesaghi, A., Yang, H., Falconieri, V., Rao, P., Merk, A., Eng, E.T., Raczkowski, A.M., Fox, T., Earl, L.A., et al. (2017). Cryo-EM Structures Reveal Mechanism and Inhibition of DNA Targeting by a CRISPR-Cas Surveillance Complex. Cell *171*, 414–426.

Gussow, A.B., Shmakov, S.A., Makarova, K.S., Wolf, Y.I., Bondy-Denomy, J., and Koonin, E.V. (2020). Vast diversity of anti-CRISPR proteins predicted with a machine-learning approach. bioRxiv. https://doi.org/10.1101/2020.01.23.916767.

Han, S., Arvai, A.S., Clancy, S.B., and Tainer, J.A. (2001). Crystal structure and novel recognition motif of rho ADP-ribosylating C3 exoenzyme from *Clostridium botulinum*: structural insights for recognition specificity and catalysis. J. Mol. Biol. *305*, 95–107.

Harrington, L.B., Doxzen, K.W., Ma, E., Liu, J.J., Knott, G.J., Edraki, A., Garcia, B., Amrani, N., Chen, J.S., Cofsky, J.C., et al. (2017). A Broad-Spectrum Inhibitor of CRISPR-Cas9. Cell *170*, 1224–1233.

Please cite this article in press as: Niu et al., A Type I-F Anti-CRISPR Protein Inhibits the CRISPR-Cas Surveillance Complex by ADP-Ribosylation, Molecular Cell (2020), https://doi.org/10.1016/j.molcel.2020.09.015



Haurwitz, R.E., Jinek, M., Wiedenheft, B., Zhou, K., and Doudna, J.A. (2010). Sequence- and structure-specific RNA processing by a CRISPR endonuclease. Science *329*, 1355–1358.

He, F., Bhoobalan-Chitty, Y., Van, L.B., Kjeldsen, A.L., Dedola, M., Makarova, K.S., Koonin, E.V., Brodersen, D.E., and Peng, X. (2018). Anti-CRISPR proteins encoded by archaeal lytic viruses inhibit subtype I-D immunity. Nat. Microbiol. *3*, 461–469.

Holm, L. (2019). Benchmarking fold detection by DaliLite v.5. Bioinformatics *35*, 5326–5327.

Hong, S., Ka, D., Yoon, S.J., Suh, N., Jeong, M., Suh, J.Y., and Bae, E. (2018). CRISPR RNA and anti-CRISPR protein binding to the *Xanthomonas albilineans* Csy1-Csy2 heterodimer in the type I-F CRISPR-Cas system. J. Biol. Chem. *293*, 2744–2754.

Hopp, A.K., Grüter, P., and Hottiger, M.O. (2019). Regulation of Glucose Metabolism by NAD(+) and ADP-Ribosylation. Cells *8*, 890.

Hu, M., Liu, Y., Yu, K., and Liu, X. (2014). Decreasing the amount of trypsin in in-gel digestion leads to diminished chemical noise and improved protein identifications. J. Proteomics *109*, 16–25.

Hwang, S., and Maxwell, K.L. (2019). Meet the Anti-CRISPRs: Widespread Protein Inhibitors of CRISPR-Cas Systems. CRISPR J. *2*, 23–30.

Hynes, A.P., Rousseau, G.M., Lemay, M.L., Horvath, P., Romero, D.A., Fremaux, C., and Moineau, S. (2017). An anti-CRISPR from a virulent streptococcal phage inhibits *Streptococcus pyogenes* Cas9. Nat. Microbiol. *2*, 1374–1380.

Hynes, A.P., Rousseau, G.M., Agudelo, D., Goulet, A., Amigues, B., Loehr, J., Romero, D.A., Fremaux, C., Horvath, P., Doyon, Y., et al. (2018). Widespread anti-CRISPR proteins in virulent bacteriophages inhibit a range of Cas9 proteins. Nat. Commun. *9*, 2919.

Knott, G.J., Thornton, B.W., Lobba, M.J., Liu, J.J., Al-Shayeb, B., Watters, K.E., and Doudna, J.A. (2019). Broad-spectrum enzymatic inhibition of CRISPR-Cas12a. Nat. Struct. Mol. Biol. *26*, 315–321.

Koonin, E.V., and Makarova, K.S. (2018). Anti-CRISPRs on the march. Science *362*, 156–157.

Lee, J., Mir, A., Edraki, A., Garcia, B., Amrani, N., Lou, H.E., Gainetdinov, I., Pawluk, A., Ibraheim, R., Gao, X.D., et al. (2018). Potent Cas9 Inhibition in Bacterial and Human Cells by AcrIIC4 and AcrIIC5 Anti-CRISPR Proteins. MBio *9*, e02321-18.

Lin, P., Qin, S., Pu, Q., Wang, Z., Wu, Q., Gao, P., Schettler, J., Guo, K., Li, R., Li, G., et al. (2020). CRISPR-Cas13 Inhibitors Block RNA Editing in Bacteria and Mammalian Cells. Mol. Cell *78*, 850–861.e5.

Liu, L., Yin, M., Wang, M., and Wang, Y. (2019). Phage AcrIIA2 DNA Mimicry: Structural Basis of the CRISPR and Anti-CRISPR Arms Race. Mol. Cell *73*, 611–620.

Mahendra, C., Christie, K.A., Osuna, B.A., Pinilla-Redondo, R., Kleinstiver, B.P., and Bondy-Denomy, J. (2020). Broad-spectrum anti-CRISPR proteins facilitate horizontal gene transfer. Nat. Microbiol. *5*, 620–629.

Makarova, K.S., Wolf, Y.I., Alkhnbashi, O.S., Costa, F., Shah, S.A., Saunders, S.J., Barrangou, R., Brouns, S.J., Charpentier, E., Haft, D.H., et al. (2015). An updated evolutionary classification of CRISPR-Cas systems. Nat. Rev. Microbiol. *13*, 722–736.

Marino, N.D., Zhang, J.Y., Borges, A.L., Sousa, A.A., Leon, L.M., Rauch, B.J., Walton, R.T., Berry, J.D., Joung, J.K., Kleinstiver, B.P., and Bondy-Denomy, J. (2018). Discovery of widespread type I and type V CRISPR-Cas inhibitors. Science *362*, 240–242.

Marino, N.D., Pinilla-Redondo, R., Csörgő, B., and Bondy-Denomy, J. (2020). Anti-CRISPR protein applications: natural brakes for CRISPR-Cas technologies. Nat. Methods *17*, 471–479.

Marraffini, L.A. (2015). CRISPR-Cas immunity in prokaryotes. Nature *526*, 55–61.

O'Sullivan, J., Tedim Ferreira, M., Gagné, J.P., Sharma, A.K., Hendzel, M.J., Masson, J.Y., and Poirier, G.G. (2019). Emerging roles of eraser enzymes in the dynamic control of protein ADP-ribosylation. Nat. Commun. *10*, 1182.

Otwinowski, Z., and Minor, W. (1997). Processing of X-ray diffraction data collected in oscillation mode. Methods Enzymol. *276*, 307–326.

Pawluk, A., Bondy-Denomy, J., Cheung, V.H.W., Maxwell, K.L., and Davidson, A.R. (2014). A new group of phage anti-CRISPR genes inhibits the type I-E CRISPR-Cas system of Pseudomonas aeruginosa. MBio *5*, e00896.

Pawluk, A., Amrani, N., Zhang, Y., Garcia, B., Hidalgo-Reyes, Y., Lee, J., Edraki, A., Shah, M., Sontheimer, E.J., Maxwell, K.L., and Davidson, A.R. (2016a). Naturally Occurring Off-Switches for CRISPR-Cas9. Cell *167*, 1829–1838.e9.

Pawluk, A., Staals, R.H., Taylor, C., Watson, B.N., Saha, S., Fineran, P.C., Maxwell, K.L., and Davidson, A.R. (2016b). Inactivation of CRISPR-Cas systems by anti-CRISPR proteins in diverse bacterial species. Nat. Microbiol. *1*, 16085.

Pawluk, A., Davidson, A.R., and Maxwell, K.L. (2018). Anti-CRISPR: discovery, mechanism and function. Nat. Rev. Microbiol. *16*, 12–17.

Peng, R., Xu, Y., Zhu, T., Li, N., Qi, J., Chai, Y., Wu, M., Zhang, X., Shi, Y., Wang, P., et al. (2017). Alternate binding modes of anti-CRISPR viral suppressors AcrF1/2 to Csy surveillance complex revealed by cryo-EM structures. Cell Res. *27*, 853–864.

Pickar-Oliver, A., Black, J.B., Lewis, M.M., Mutchnick, K.J., Klann, T.S., Gilcrest, K.A., Sitton, M.J., Nelson, C.E., Barrera, A., Bartelt, L.C., et al. (2019). Targeted transcriptional modulation with type I CRISPR-Cas systems in human cells. Nat. Biotechnol. *37*, 1493–1501.

Przybilski, R., Richter, C., Gristwood, T., Clulow, J.S., Vercoe, R.B., and Fineran, P.C. (2011). Csy4 is responsible for CRISPR RNA processing in *Pectobacterium atrosepticum*. RNA Biol. *8*, 517–528.

Qi, H., Price, B.D., and Day, T.A. (2019). Multiple Roles for Mono- and Poly(ADP-Ribose) in Regulating Stress Responses. Trends Genet. *35*, 159–172.

Rauch, B.J., Silvis, M.R., Hultquist, J.F., Waters, C.S., McGregor, M.J., Krogan, N.J., and Bondy-Denomy, J. (2017). Inhibition of CRISPR-Cas9 with Bacteriophage Proteins. Cell *168*, 150–158.e10.

Rollins, M.F., Chowdhury, S., Carter, J., Golden, S.M., Miettinen, H.M., Santiago-Frangos, A., Faith, D., Lawrence, C.M., Lander, G.C., and Wiedenheft, B. (2019). Structure Reveals a Mechanism of CRISPR-RNA-Guided Nuclease Recruitment and Anti-CRISPR Viral Mimicry. Mol. Cell *74*, 132–142.

Schindelin, J., Rueden, C.T., Hiner, M.C., and Eliceiri, K.W. (2015). The ImageJ ecosystem: An open platform for biomedical image analysis. Mol. Reprod. Dev. *82*, 518–529.

Shniffer, A., Visschedyk, D.D., Ravulapalli, R., Suarez, G., Turgeon, Z.J., Petrie, A.A., Chopra, A.K., and Merrill, A.R. (2012). Characterization of an actin-targeting ADP-ribosyltransferase from *Aeromonas hydrophila*. J. Biol. Chem. *287*, 37030–37041.

Simon, N.C., Aktories, K., and Barbieri, J.T. (2014). Novel bacterial ADP-ribosylating toxins: structure and function. Nat. Rev. Microbiol. *12*, 599–611.

Uribe, R.V., van der Helm, E., Misiakou, M.A., Lee, S.W., Kol, S., and Sommer, M.O.A. (2019). Discovery and Characterization of Cas9 Inhibitors Disseminated across Seven Bacterial Phyla. Cell Host Microbe *25*, 233–241.e5.

van der Oost, J., Westra, E.R., Jackson, R.N., and Wiedenheft, B. (2014). Unravelling the structural and mechanistic basis of CRISPR-Cas systems. Nat. Rev. Microbiol. *12*, 479–492.

Wang, J., Ma, J., Cheng, Z., Meng, X., You, L., Wang, M., Zhang, X., and Wang, Y. (2016a). A CRISPR evolutionary arms race: structural insights into viral anti-CRISPR/Cas responses. Cell Res. *26*, 1165–1168.

Wang, X., Yao, D., Xu, J.G., Li, A.R., Xu, J., Fu, P., Zhou, Y., and Zhu, Y. (2016b). Structural basis of Cas3 inhibition by the bacteriophage protein AcrF3. Nat. Struct. Mol. Biol. *23*, 868–870.

Wang, Q.-S., Zhang, K.-H., Cui, Y., Wang, Z.-J., Pan, Q.-Y., Liu, K., Sun, B., Zhou, H., Li, M.-J., Xu, Q., et al. (2018). Upgrade of macromolecular crystallography beamline BL17U1 at SSRF. Nucl. Sci. Tech. *29*, 68.

Please cite this article in press as: Niu et al., A Type I-F Anti-CRISPR Protein Inhibits the CRISPR-Cas Surveillance Complex by ADP-Ribosylation, Molecular Cell (2020), https://doi.org/10.1016/j.molcel.2020.09.015



Watters, K.E., Fellmann, C., Bai, H.B., Ren, S.M., and Doudna, J.A. (2018). Systematic discovery of natural CRISPR-Cas12a inhibitors. Science *362*, 236–239.

Watters, K.E., Shivram, H., Fellmann, C., Lew, R.J., McMahon, B., and Doudna, J.A. (2020). Potent CRISPR-Cas9 inhibitors from *Staphylococcus* genomes. Proc. Natl. Acad. Sci. USA *117*, 6531–6539.

Zhang, F., Zhao, S., Ren, C., Zhu, Y., Zhou, H., Lai, Y., Zhou, F., Jia, Y., Zheng, K., and Huang, Z. (2018). CRISPRminer is a knowledge base for exploring CRISPR-Cas systems in microbe and phage interactions. Commun. Biol. *1*, 180.

Zhang, H., Li, Z., Daczkowski, C.M., Gabel, C., Mesecar, A.D., and Chang, L. (2019a). Structural Basis for the Inhibition of CRISPR-Cas12a by Anti-CRISPR Proteins. Cell Host Microbe *25*, 815–826.e4.

Zhang, W.-Z., Tang, J.-C., Wang, S.-S., Wang, Z.-J., Qin, W.-M., and He, J.-H. (2019b). The protein complex crystallography beamline (BL19U1) at the Shanghai Synchrotron Radiation Facility. Nucl. Sci. Tech. *30*, 170.

Zhang, K., Wang, S., Li, S., Zhu, Y., Pintilie, G.D., Mou, T.C., Schmid, M.F., Huang, Z., and Chiu, W. (2020). Inhibition mechanisms of AcrF9, AcrF8, and AcrF6 against type I-F CRISPR-Cas complex revealed by cryo-EM. Proc. Natl. Acad. Sci. USA *117*, 7176–7182.

Zhou, Y., Wang, L., Yang, F., Lin, X., Zhang, S., and Zhao, Z.K. (2011). Determining the extremes of the cellular NAD(H) level by using an *Escherichia coli* NAD(+)-auxotrophic mutant. Appl. Environ. Microbiol. *77*, 6133–6140.

Please cite this article in press as: Niu et al., A Type I-F Anti-CRISPR Protein Inhibits the CRISPR-Cas Surveillance Complex by ADP-Ribosylation, Molecular Cell (2020), https://doi.org/10.1016/j.molcel.2020.09.015



## STAR★METHODS

### KEY RESOURCES TABLE

| REAGENT or RESOURCE | SOURCE | IDENTIFIER |
|---|---|---|
| Antibodies | | |
| pan-ADP-ribose-recognizing antibody | Homemade | N/A |
| HRP-Streptavidin | Beyotime | Cat#A0303 |
| Anti-Flag Monoclonal Antibody | BIODEE | Cat#DE0611 |
| Bacterial and Virus Strains | | |
| *E. coli*: BL21(DE3) Competent cell | Transgen Biotech | CD601-02 |
| *E. coli*: Trans5α Competent Cell | Transgen Biotech | CD201-01 |
| *P. aeruginosa* PA14 Competent Cell | Homemade | N/A |
| Chemicals, Peptides, and Recombinant Proteins | | |
| HEPES sodium salt | VETEC | CAS:7365-45-9. Cat#V900477-500G |
| Sodium citrate tribasic dihydrate | VETEC | CAS:6132-04-3. Cat#V900095-500G |
| β-nicotinamide adenine dinucleotide | Sigma-Aldrich | CAS:53-84-9. Cat#N7004 |
| Biotin-NAD | TREVIGEN | Cat#4670-500-01 |
| L(+)-Selenomethionine (Se-Met) | Acros | CAS:3211-76-5. Cat#259960025 |
| PrimeSTAR Max | Takara | Cat#R045 |
| T5 Super PCR Mix | TSINGKE | Cat#TSE005 |
| Dpn I | NEB | Cat#R0176s |
| KOD-Plus-Neo | TOYOBO | Cat#KOD-401 |
| High Affinity Ni-NTA Resin | GenScript | Cat#L00250-100 |
| Phenazine ethosulfate | Shanghai yuanye Bio-Technology | CAS:10510-77-7. Cat#S30739-1G |
| Thiazolyl blue tetrazolium bromide | MACKLIN | CAS:298-93-1. Cat#T818538-1g |
| Alcohol dehydrogenase | Shanghai yuanye Bio-Technology | CAS:9031-72-5. Cat#S10110-7.5KU |
| Nicotinamide 1, N6-ethenoadenine dinucleotide | Sigma-Aldrich | CAS:38806-38-1. Cat#N2630-5MG |
| Critical Commercial Assays | | |
| Plasmid Miniprep Kit | ZOMANBIO | Cat#ZP101-3 |
| DNA Gel Extraction Kit | AXYGEN | Cat#AP-GX-250 |
| Deposited Data | | |
| Structure of AcrIF11 | This paper | PDB: 6KYF |
| Recombinant DNA | | |
| pGEX6p-1-GST-AcrIF2 | This paper | N/A |
| pGEX6p-1-GST-AcrIF3 | This paper | N/A |
| pGEX6p-1-GST-AcrIF5 | This paper | N/A |
| pGEX6p-1-GST-AcrIF6 | This paper | N/A |
| pGEX6p-1-GST-AcrIF7 | This paper | N/A |
| pGEX6p-1-GST-AcrIF8 | This paper | N/A |
| pGEX6p-1-GST-AcrIF9 | This paper | N/A |
| pGEX6p-1-GST-AcrIF10 | This paper | N/A |
| pGEX6p-1-GST-AcrIF11 | This paper | N/A |
| pGEX6p-1-GST-AcrIF11-H7A/S9A/E11A | This paper | N/A |
| pGEX6p-1-GST-AcrIF11-H7A/F26A | This paper | N/A |
| pGEX6p-1-GST-AcrIF11-H7A/H117A | This paper | N/A |
| pGEX6p-1-GST-AcrIF11-H37A/Q96A | This paper | N/A |
| pGEX6p-1-GST-AcrIF11-H37A/H117A | This paper | N/A |
| pGEX6p-1-GST-AcrIF11-D115A | This paper | N/A |

(*Continued on next page*)

Please cite this article in press as: Niu et al., A Type I-F Anti-CRISPR Protein Inhibits the CRISPR-Cas Surveillance Complex by ADP-Ribosylation, Molecular Cell (2020), https://doi.org/10.1016/j.molcel.2020.09.015



*Continued*

| REAGENT or RESOURCE | SOURCE | IDENTIFIER |
|---|---|---|
| pUCP19-AcrIF11-FLAG | This paper | N/A |
| pET22b-AcrIF11-1-50, 108-132 | This paper | N/A |
| pGEX6p-1-GST-AcrIF13 | This paper | N/A |
| pGEX6p-1-GST-AcrIF14 | This paper | N/A |
| pET-Duet-1-Cas8f-Cas5f | This paper | N/A |
| pET-Duet-1-Cas8f-K247A-Cas5f | This paper | N/A |
| pET-Duet-1-Cas8f-K247E-Cas5f | This paper | N/A |
| pET-Duet-1-Cas8f-N250A-Cas5f | This paper | N/A |
| pET-Duet-1-Cas8f-N250D-Cas5f | This paper | N/A |
| pACYCDuet-1-$His_6$-Cas7f-Cas6f | This paper | N/A |
| pACYCDuet-1-$His_6$-Cas7f-S54A/N55A-Cas6f | This paper | N/A |
| pACYCDuet-1-$His_6$-Cas7f-K58A/K60A-Cas6f | This paper | N/A |
| pACYCDuet-1-$His_6$-Cas7f-K58A-Cas6f | This paper | N/A |
| pACYCDuet-1-$His_6$-Cas7f-K60A-Cas6f | This paper | N/A |
| pACYCDuet-1-$His_6$-Cas7f-K66A/S70A-Cas6f | This paper | N/A |
| pACYCDuet-1-$His_6$-Cas7f-Q241A/K242A-Cas6f | This paper | N/A |
| pACYCDuet-1-$His_6$-Cas7f-Q291A/K293A-Cas6f | This paper | N/A |
| pACYCDuet-1-$His_6$-Cas7f-Q297A/K299A-Cas6f | This paper | N/A |
| pACYCDuet-1-$His_6$-Cas7f-V335A/E338A-Cas6f | This paper | N/A |
| pRSFDuet-1-crRNA | This paper | N/A |
| pETDuet-1-GST-Cas2/3 | This paper | N/A |
| Software and Algorithms | | |
| HKL2000 | Otwinowski and Minor, 1997 | http://www.hkl-xray.com/ |
| Phenix | Adams et al., 2002 | http://www.phenix-online.org |
| COOT | Emsley et al., 2010 | http://www2.mrc-lmb.cam.ac.uk/personal/pemsley/coot |
| PyMOL | The PyMOL Molecular Graphics System, Version 1.8.4.0, Schrodinger, LLC | https://pymol.org/2/ |
| OriginPro 8 | OriginPro software | N/A |
| GraphPad Prism 8 | GraphPad Software | https://www.graphpad.com/ |
| ImageJ | Schindelin et al., 2015 | https://imagej.net/Welcome |
| Other | | |
| Amicon concentrators (10K) | Millipore | Cat#UFC901096 |
| Amicon concentrators (30K) | Millipore | Cat#UFC903024 |
| HisTrap FF (5 mL) | GE Healthcare | Cat#17-5255-01 |
| HiTrap Heparin HP (5 mL) | GE Healthcare | Cat#17-0407-03 |
| HiTrap Q Sepharose FF (5 mL) | GE Healthcare | Cat#17-5156-01 |
| Superdex 75 10/300 GL | GE Healthcare | Cat#17517401 |
| Superdex 200 10/300 GL | GE Healthcare | Cat#17517501 |
| Glutathione Sepharose 4B | GE Healthcare | Cat#45-000-139 |

## RESOURCE AVAILABILITY

### Lead Contact

Further information and requests for resources and reagents should be directed to and will be fulfilled by the Lead Contact, Yue Feng (fengyue@mail.buct.edu.cn).

Please cite this article in press as: Niu et al., A Type I-F Anti-CRISPR Protein Inhibits the CRISPR-Cas Surveillance Complex by ADP-Ribosylation, Molecular Cell (2020), https://doi.org/10.1016/j.molcel.2020.09.015



### Materials Availability

All unique/stable reagents generated in this study are available from the Lead Contact with a completed Materials Transfer Agreement.

### Data and Code Availability

The accession number for the coordinate and structure factors reported in this paper is PDB: 6KYF (AcrIF11).

## EXPERIMENTAL MODEL AND SUBJECT DETAILS

Recombinant proteins were overexpressed in *Escherichia coli* BL21 (DE3) strain in Lysogeny broth (LB) medium. The cells were grown at 37°C until $OD_{600nm}$ reached 0.8 and then induced at 16°C for 12 h.

## METHOD DETAILS

### Protein expression and purification

The full-length AcrIF2, AcrIF3, AcrIF5-F10 and AcrIF11-F14 genes were synthesized by GenScript and amplified by PCR and cloned into pGEX6p-1 to produce GST-tagged fusion proteins with a PreScission Protease cleavage site between GST and the target proteins. The AcrIF11 mutants were generated by two-step PCR and were subcloned, overexpressed and purified in the same way as wild-type protein. The proteins were expressed in *E. coli* strain BL21 (DE3) and induced by 0.2 mM isopropyl-β-D-thiogalactopyranoside (IPTG) when the cell density reached an $OD_{600nm}$ of 0.8. After growth at 16°C for 12 h, the cells were harvested, re-suspended in lysis buffer (1 × PBS, 2 mM DTT and 1 mM PMSF) and lysed by sonication. The cell lysate was centrifuged at 20,000 g for 45 min at 4°C to remove cell debris. The supernatant was applied onto a self-packaged GST-affinity column (2 mL glutathione Sepharose 4B; GE Healthcare) and contaminant proteins were removed with wash buffer (lysis buffer plus 200 mM NaCl). The fusion protein was then digested with PreScission protease at 4°C overnight. The protein with an additional five-amino-acid tag (GPLGS) at the N terminus was eluted with lysis buffer. The eluant was concentrated and further purified using a Superdex-75 (GE Healthcare) column equilibrated with a buffer containing 10 mM Tris–HCl pH 8.0, 200 mM NaCl, and 5 mM DTT. The purified protein was analyzed by SDS–PAGE. Selenomethionine (Se-Met)-labeled AcrIF11 was expressed in *E. coli* BL21 cells grown in M9 minimal medium supplemented with 35 mg/L Se-Met (Acros) and specific amino acids: Ile, Leu and Val at 50 mg/L; Lys, Phe and Thr at 100 mg/L. The SeMet protein was purified as described above.

The Csy complex from *Pseudomonas aeruginosa* was purified as follows. The Cas8f/Cas5f and Cas7f/Cas6f genes were cloned into pETDuet-1 and pACYCDuet-1, respectively. The crRNA fragment was cloned into pRSFDuet-1 vector. After co-expression of the three plasmids in *E. coli* strain BL21, the Csy complex was purified through Ni-column, anion exchange chromatography and gel filtration. The mutations of Cas8f and Cas7f were made as above and the Csy complex with Cas8f and Cas7f mutations were purified similarly as the wild-type complex.

The Cas2/3 gene was cloned into a modified pETDuet-1 vector with a GST tag at the N terminus of the protein and transformed into *E. coli* strain BL21. The protein was purified through GST column as stated above, and then by heparin chromatography and gel filtration.

The DNA for AcrIF11Δα (1-50, 108-132 residues) was cloned into pET22b vector with a C-terminal His tag and purified as above described for the Csy complex.

### Crystallization, data collection and structure determination

The AcrIF11 was concentrated to 10 mg/mL in 10 mM Tris-HCl pH 8.0, 200 mM NaCl and 5 mM DTT. Crystals were grown using the hanging-drop vapor diffusion method. Crystals of AcrIF11 were grown at 18°C by mixing an equal volume of the protein (10mg/mL) with reservoir solution containing 0.1 M HEPES pH 7.5, 1.4 M Sodium citrate tribasic dihydrate and 20 mM β-$NAD^+$. The crystals appeared overnight and grew to full size in about four to five days. The crystals were cryoprotected in the reservoir solution containing 10% glycerol before its transferring to liquid nitrogen. Se-Met-labeled protein was crystallized in the same buffer, and the crystals diffracted better than the native one. After crystal diffraction tests at home and beamlines BL17U1 and BL19U1 of the Shanghai Synchrotron Radiation Facility (SSRF), the crystal of the Se-Met-labeled protein suitable for structure determination was finally obtained.

All the data were collected at SSRF beamlines BL17U1 (Wang et al., 2018) and BL19U1 (Zhang et al., 2019b), integrated and scaled using the HKL2000 package (Otwinowski and Minor, 1997). The initial model was solved by Autosol in PHENIX (Adams et al., 2002) and refined manually using COOT (Emsley et al., 2010). The structure was further refined with PHENIX (Adams et al., 2002) against the native data using non-crystallographic symmetry and stereochemistry information as restraints. The final structure was obtained through several rounds of refinement. Data collection and structure refinement statistics are summarized in Table 1. All of the structural illustrations were generated using the software PyMOL.

### In vitro DNA cleavage assay

Non-target DNA strand with 5′ end FAM labeling was purchased from Sangon, Shanghai. Target and non-target DNA strands were hybridized with a molar ratio of 1.5:1 to obtain a dsDNA. For testing the activity of AcrIF11 and its mutants, reactions were performed

Please cite this article in press as: Niu et al., A Type I-F Anti-CRISPR Protein Inhibits the CRISPR-Cas Surveillance Complex by ADP-Ribosylation, Molecular Cell (2020), https://doi.org/10.1016/j.molcel.2020.09.015





in a 20 μL buffer system containing 0.8 μM Csy complex, 40 nM dsDNA, and 2.4 μM AcrIF11 or its mutants. NAD was added with a concentration of 25 μM when needed. We first incubated AcrIF11 or AcrIF11 mutants with Csy in ice in reaction buffer (20 mM HEPES pH 7.5, 100 mM KCl, 5% glycerol, 1 mM TCEP) for 30 min, and DNA was added and incubated for another 15 min. And then Cas2/3 was added to a final concentration of 0.4 μM, along which 5 mM $MgCl_2$, 75 μM $NiSO_4$, 5 mM $CaCl_2$, and 1 mM ATP were added into the buffer. The reaction was further incubated for 15 min and quenched with 1% SDS and 8 mM EDTA. The products were separated by electrophoresis over 14% polyacrylamide gels containing 7 M urea and visualized by fluorescence imaging. For testing the activity of AcrIF11 and other Acr proteins, Acr proteins were added with concentrations of 2.4 μM, 0.24 μM, 24 nM and 2.4 nM, respectively. The experimental procedure was basically the same as above, except that Acr proteins were incubated with the Csy complex at 37°C in the above reaction buffer.

Non-Target DNA sequence (54 bp; 5′-FAM fluorescein labeled)
AGCAGCTGCACCTTCACGGCGGGCTTGATGTCCGCGTCTACCTGGATGGCTTCC

### Gel filtration assay

All the proteins involved were purified as described above. The Csy complex/Cas2-3 and the Acr proteins, with a molar ratio of 1:5, were incubated in ice overnight. The incubation samples were applied to a size-exclusion chromatography column (Superdex-200 increase 10/300 GL, or Superdex-75 increase 10/300 GL, GE Healthcare) equilibrated with a buffer containing 10 mM Tris-HCl pH 8.0, 200 mM NaCl, and 5 mM DTT. The assays were performed with a flow rate of 0.5 mL/min and an injection volume of 1 mL for each run. Samples taken from relevant fractions were applied to SDS-PAGE and visualized by Coomassie blue staining.

### Electrophoretic mobility shift assay

Target DNA strand with 5′ end FAM labeling was purchased from Sangon, Shanghai. Target and non-target DNA strands were hybridized with a molar ratio of 1:1.5 to obtain a dsDNA. Reactions were performed in a 20 μL buffer system containing 8 μM Csy complex, 0.5 μM dsDNA, 32 μM AcrIF11 or its mutants. NAD was added with a concentration of 50 μM when needed. All binding reactions were conducted at 37°C for 30 min in the buffer containing 20 mM HEPES pH 7.5, 150 mM NaCl and 5% glycerol. Products of the reaction were separated using 5% native polyacrylamide gels and visualized by fluorescence imaging.

For binding affinity, the Csy complex was incubated in a concentration gradient (0, 0.003125, 0.03125, 0.15625, 0.3125, 1.5625, 3.125, 31.25, 312.5, 3125, 31250 nM) with 6.25 nM of 54 bp-dsDNA (5′-FAM in the TS). The molar ratio of AcrIF11/NAD to Csy was 4:1, when needed. All binding reactions were conducted at 37°C for 30 min in the buffer containing 20 mM HEPES pH 7.5, 100 mM KCl, 5% glycerol and 1 mM TCEP. Products of the reaction were separated using 5% native polyacrylamide gels and visualized by fluorescence imaging. The fluorescence signal was measured using ImageJ (Schindelin et al., 2015). The bound DNA was quantified and the binding curves were fitted to a one specific binding site model with Prism (GraphPad Software).

Target DNA sequence (54 bp; 5′-FAM fluorescein labeled)
GGAAGCCATCCAGGTAGACGCGGACATCAAGCCCGCCGTGAAGGTGCAGCTGCT

### In-gel protein digestion and LC-MS/MS analyses

The Csy complex was co-expressed with AcrIF11, purified to homogeneity and subjected to SDS-PAGE. The target band was cut off and subjected to in-gel trypsin digestion as previously described (Hu et al., 2014). The resulting peptides were reconstituted in HPLC-grade water for LC-MS/MS analyses on an ion trap mass spectrometer (LTQ Velos Pro, Thermo Scientific) coupled with nanoflow reversed-phase liquid chromatography (EASY-nLC 1200, Thermo Scientific). The capillary column (75 μm × 150 mm) with a laser-pulled electrospray tip (Model P-2000, Sutter Instruments) was home-packed with 5 μm, 100 Å Magic C18AQ silica-based particles (Michrom BioResources Inc., Auburn, CA) and run at 300 nL/min with the following mobile phases (A: 97% water, 3% acetonitrile, and 0.1% formic acid; B: 80% acetonitrile, 20% water, and 0.1% formic acid). The LC gradient started at 7% B for 3 min and then was linearly increased to 37% in 40 min. Next, the gradient was quickly ramped to 95% in 2 min and stayed there for 10 min. The gradient was then switched back to 100% solvent A for column equilibration. Eluted peptides from the capillary column were electrosprayed directly onto the mass spectrometer for MS and MS/MS analyses in a data-dependent acquisition mode. One full MS scan (m/z 350-1500) was acquired and subsequently the ten most intense ions were selected and fragmented by collision-induced dissociation (CID). Dynamic exclusion was set with repeat duration of 12 s and exclusion duration of 6 s. To identify potential modification sites, LC-MS/MS analyses were carried on a hybrid ion trap-Orbitrap mass spectrometer (LTQ Orbitrap Elite, Thermo Scientific) and fragmented by electron transfer dissociation (ETD).

### In vitro modification assay

The reactions were performed in a 20 μL buffer system containing 0.48 μM Csy complex or its mutants, 2.4 μM wild-type AcrIF11 or its mutants, and 10 μM biotin-NAD. For the reactions with NAD, they were performed in a 20 μL buffer system containing 8 μM Csy complex or Cas2/3, 32 μM wild-type AcrIF11, and 100 μM NAD. All the reactions were conducted at 37°C for 120 min in the buffer containing 10 mM Tris-HCl (pH 8.0), 200 mM NaCl, and 5 mM DTT. After the reaction, the samples were subjected to SDS-PAGE gels. The gels were then blotted on nitrate cellulose strips (Sartorius Stedim #11327-41BL) in standard blotting buffer. Blocking of the immunoblot was done in 5% milk in TBS-Tween20. For the reactions with biotin-NAD, the antibody used for immunoblot analysis was HRP-Streptavidin (Beyotime, A0303). For the reactions with NAD, the antibody used was pan-ADP-ribose-recognizing antibody.

Please cite this article in press as: Niu et al., A Type I-F Anti-CRISPR Protein Inhibits the CRISPR-Cas Surveillance Complex by ADP-Ribosylation, Molecular Cell (2020), https://doi.org/10.1016/j.molcel.2020.09.015



### Isothermal titration calorimetry binding assay

The dissociation constants of binding reactions of AcrIF11 or AcrIF11 mutants with β-NAD were determined by isothermal titration calorimetry (ITC) using a MicroCal ITC200 calorimeter. Both proteins and β-NAD were desalted into the working buffer (20 mM HEPES pH 7.5 and 200 mM NaCl). The titration was carried out with 19 successive injections of 2 μL β-NAD at the 1 mM concentration, spaced 120 s apart, into the sample cell containing the AcrIF11 or its mutants (residues 1-134) at the 0.05 mM concentration by 750 rpm at 25°C. The dissociation constant of binding reaction of AcrIF11 or its mutants with the Csy complex or its mutants was determined similarly. All the proteins involved were desalted into the same working buffer as above. The titration was carried out with 19 successive injections of 2 μL AcrIF11 at the 0.5 mM concentration, spaced 120 s apart, into the sample cell containing the Csy complex or its mutants at the 0.04 mM concentration by 500 rpm at 25°C. The Origin software was used for baseline correction, integration, and curve fitting to a single site binding model.

### Enzymatic kinetics assay of AcrIF11

Kinetic assays were performed following a slightly modified protocol as previously described (Shniffer et al., 2012). In brief, 0.5 μM AcrIF11 was incubated with varied concentrations of the Csy complex (ranging from 4 to 64 μM) and 300 μM ε-$NAD^+$ to determine the $K_m$ and $k_{cat}$. Increasing fluorescence intensity was recorded as the reaction progressed (excitation wavelength: 300 nm, emission wavelength: 410 nm) on an Enspire multimode plate reader, PerkinElmer. All reactions were performed at 37°C in 50 mM Tris-HCl, pH 7.5, 10 mM NaCl. Calibration curves was created by measuring fluorescence intensity changes upon completion of the reaction at various Csy complex concentrations in the presence of excess ε-$NAD^+$, and by assuming the molar amounts of Csy complex and ε-$NAD^+$ consumed by the reaction are equal.

### Expression of AcrIF11 in Pseudomonas aeruginosa PA14 and $NAD^+$ quantification

The AcrIF11 gene was cloned into the pUCP19 vector with a C-terminal FLAG tag. The pUCP19 vector and the one containing AcrIF11 were transformed into competent *P. aeruginosa* cells through electroporation as described previously (Choi et al., 2006). The expression of AcrIF11 was detected through immunoblotting of the FLAG tag. Determination of $NAD^+$ level was performed according to the method reported by Zhou et al. (2011), except that the volume of the reaction system was 100 μL.

### Surface Plasmon Resonance binding assay

The SPR analysis was performed using a BIAcore 3000 machine (GE Healthcare) at room temperature (25°C). AcrIF11 was biotinylated and immobilized on a SA chip to about 280 Response Unit (RU). To collect data for kinetic analysis, a concentration series of the Csy complex in binding buffer (1 × PBS and 0.05% (v/v) Tween-20) were injected over the chip at a flow rate of 30 μL/min. The complex was allowed to associate for 60 s and dissociate for 90 s. Data was analyzed with BIAevaluation 4.1 software (GE Healthcare) by fitting to a 1:1 Langmuir binding fitting model.

### Analysis of AcrIF11-associated CRISPR systems

The genomic sequences of the bacterial genomes holding AcrIF11 homologs were downloaded from NCBI database, and the CRISPR-Cas systems on these genomes were predicted using CRISPRminer pipeline (Zhang et al., 2018).

## QUANTIFICATION AND STATISTICAL ANALYSIS

ITC data in Figures 2D, 3F, and S3 are analyzed with Origin software. Data are represented as mean ± SEM.